The Thesis Committee for Antoine Marc Marie Montaut
Certifies that this is the approved version of the following thesis:

DETECTION AND QUANTIFICATION OF ROCK PHYSICS PROPERTIES FOR IMPROVED HYDRAULIC FRACTURING IN HYDROCARBON-BEARING SHALES

APPROVED BY
SUPERVISING COMMITTEE:

Supervisor:

Carlos Torres-Verdín

Kyle Spikes

DETECTION AND QUANTIFICATION OF ROCK PHYSICS PROPERTIES FOR IMPROVED HYDRAULIC FRACTURING IN HYDROCARBON-BEARING SHALES

by

Antoine Marc Marie Montaut, B.S.E

Thesis

Presented to the Faculty of the Graduate School of

The University of Texas at Austin

in Partial Fulfillment

of the Requirements

for the Degree of

Master of Science in Engineering

The University of Texas at Austin

December 2012

Dedication

I dedicate this thesis to my family.

Acknowledgements

I would like to thank Dr. Carlos Torres-Verdín for his devotion to his students and his assistance with my project. He taught me the importance of being rigorous in every aspect of my work, and he emphasized the need for seeking physical meaning behind every phenomenon. I also thank Dr. Spikes for accepting to by my second reader and for his valuable insights.

I am grateful to Nigel Quayle and Sylviane Wignacourt for helping me join this program. They have shown me continuous kindness and support throughout this experience.

I thank my fellow students from the Formation Evaluation group for their support, their friendship, and their technical expertise. I am particularly grateful to Haryanto Adiguna, Paul Sayar, Philippe Marouby, Andy Popielski, Siddarth Misra, and Elton Ferreira.

My thanks also go to the Petroleum and Geosystems Engineering faculty, especially to Rey Casanova for his support and assistance. I am also grateful to Frankie Hart for their kindness and help.

For their continuous love, I thank my family. They have been supporting me since the very beginning, and I could not have completed this degree without them.

The work reported in this paper was funded by The University of Texas at Austin's Research Consortium on Formation Evaluation, jointly sponsored by Anadarko, Apache, Aramco, Baker-Hughes, BG, BHP Billiton, BP, Chevron, China Oilfield Services, LTD., ConocoPhillips, ENI, ExxonMobil, Halliburton, Hess, Maersk, Marathon Oil Corporation, Mexican Institute for Petroleum, Nexen, ONGC, Petrobras, Repsol,

RWE, Schlumberger, Shell, Statoil, Total, Weatherford and Woodside Petroleum Limited.

Abstract

DETECTION AND QUANTIFICATION OF ROCK PHYSICS PROPERTIES FOR IMPROVED HYDRAULIC FRACTURING IN HYDROCARBON-BEARING SHALES

Antoine Marc Marie Montaut, M.S.E.

The University of Texas at Austin, 2012

Supervisor: Carlos Torres-Verdín

Horizontal drilling and hydraulic stimulation make hydrocarbon production from organic-rich shales economically viable. Identification of suitable zones to drill a horizontal well and to initiate or contain hydraulic fractures requires detection and quantification of many factors, including elastic mechanical properties. Elastic behavior of rocks is affected by rock composition and fabric, pore pressure, confining stress, and other factors. Rock fabric refers to the arrangement of the rock's solid and fluid constituents. The objective of this thesis is to quantify rock fabric properties of hydrocarbon-bearing shales affecting elastic properties, including load-bearing matrix, anisotropic cracks, and shape of rock components. Once rock fabric is validated with

sonic logs, results can be used to identify suitable zones to drill a horizontal well, initiate hydraulic stimulation, and contain fracture propagation.

We develop a method to estimate elastic properties based on rock composition. The differential effective medium (DEM) theory is invoked to model rock elastic properties with a load-bearing component in which remaining minerals and pores are added as spheres or ellipsoids. The method can be combined with the self-consistent approximation (SCA) to construct a load-bearing matrix made of two solid phases. Anisotropic inclusions are added via Hudson's model. Subsequently, Gassmann's theory is invoked to saturate the rock with fluids and determine low-frequency elastic properties for comparison to sonic logs. Rock fabric properties remain constant in a vertically homogeneous formation. In vertically heterogeneous strata, the depth interval of interest is divided into rock types, based on rock solid composition, and each rock type is associated with a specific fabric. Quantification of rock fabric properties is a non-unique process, and one should take into account as much petrophysical and geological information as possible to ensure physically viable results.

Our simulation and interpretation method is implemented in two wells in both the Haynesville and Barnett shales. Averages of relative errors between estimated velocities and sonic logs are less than 4% in the four wells. Simulations in the Haynesville shale are isotropic, and therefore indicate that rock fabric may not be the main cause of mechanical anisotropy in cases where such behavior is inferred from field data. Rock fabric properties are constant with depth in both wells. Consequently, identification of suitable zones to drill a horizontal well or to contain fracture propagation is not based on rock

fabric; it is deduced from Young's modulus. Simulated Poisson's ratio is shown to be more sensitive to errors in velocities than Young's modulus and is therefore not used in the interpretation. Favorable depth intervals for gas production exhibit sizeable volumes of gas and organic content.

In the Barnett shale, the two wells exhibit different rock fabrics. Such a behavior indicates that the formation is laterally heterogeneous. Rock physics models should therefore be extrapolated from one well to another with caution. Simulations assume anisotropic elastic behavior and suggest the presence of compliant horizontal pores in one case. Natural vertical fractures are observed on electric image logs in the remaining case and are modeled with Hudson's theory. This behavior suggests that rock fabric causes mechanical anisotropy in the formation. Heterogeneity of the Barnett shale rock fabric is inferred from the necessary use of rock typing to adequately reproduce sonic logs in both wells. Intervals with large porosity and high gas saturation identify suitable zones to perform hydraulic stimulation. Among such zones, rock types that exhibit stiff load-bearing matrices (comprising mostly calcite, for example) indicate suitable depths to drill horizontal wells or to contain hydraulic fractures. Intervals with dense layering of different rock types are unsuitable for fracture propagation and should be avoided during hydraulic-fracturing operations.

Table of Contents

List of Tables

List of Figures

Chapter 1: Introduction

Hydrocarbon source rocks in the form of organic shales are known not only to produce hydrocarbons but also to trap these hydrocarbons, acting as potential reservoirs. Due to their very low permeability—less than 0.1 mD, as defined by the Federal Energy Regulatory Commission (FERC)—, heterogeneous mineralogy and overall complexity, these formations were, for a long time, out of reach for the petroleum industry. Hydrocarbon-bearing shales remained unproduced until the combination of horizontal drilling and hydraulic fracturing became possible and economically viable. By providing large spatial exposure and intense stimulation in rocks, these major technological breakthroughs enabled the economic production of shale gas and shale oil.

1.1 Background

Designing a horizontal well and optimizing hydraulic stimulation are complex processes that require detection and quantification of many factors such as rock composition, rock fabric, formation heterogeneity, brittleness, in-situ stress, elastic properties, pore pressure, temperature, and others (King, 2010). Affected by most of these factors, fracturability quantifies how efficiently a fracture forms and propagates in a rock. In shale gas formations, fracturability typically correlates with mineralogy (Jarvie et al., 2007) and rock elastic properties such as Young's modulus (Britt and Schoeffler, 2009), which is an isotropic elastic property. Brittle rocks, characterized by low clay content and high static Young's modulus, are more suitable for efficient hydraulic-fracture initiation and growth than are ductile rocks. Brittle rocks are also suitable for horizontal drilling because they are resistant to collapse or fracture closure; closed fractures around the wellbore suppress the advantages of hydraulic stimulation by cutting

flow paths near the well. Fracture healing and embedment are likely to take place in ductile rocks with high clay content and low static Young's modulus.

Dynamic elastic properties (including Young's modulus whenever the formation elastic properties are assumed to be isotropic) can be calculated from sonic and density logs. Static and dynamic Young moduli tend to correlate in shale gas (Britt and Schoeffler, 2009). Therefore, Young moduli estimated from sonic logs are reliable for estimation of fracturability of rocks. Only a subset of elastic tensor components is available through sonic logging in anisotropic rocks. Even though sonic measurements are often incomplete in strata with a high degree of anisotropy, the widespread use of sonic logs in the industry and research, including their use in shale gas formations, indicates the reliability of such data for fracturability quantification and elastic-property estimation.

Volumetric concentration of minerals, organic content, porosity, types of fluid, and fluid saturation can be estimated with multi-mineral nonlinear inversion of conventional well logs (Heidari, 2011). Such inversion methods estimate rock composition, but no information is provided on how individual rock components are spatially arranged and how they contribute to the bulk rock mechanical properties. How individual rock components are spatially arranged is referred as rock fabric. Rock fabric is characterized by properties such as load-bearing matrix, shapes of solid particles, shapes of pores, presence of fractures, and layering. Rocks with equal composition but different rock fabrics can exhibit different mechanical behavior, therefore different elastic properties. Due to complex solid composition, various types of porosity—from micro pores to macro fractures—, vertical variability, and other characteristics, it becomes critical to identify and quantify rock fabric parameters of shales to accurately estimate their elastic properties from sonic logs.

Many interpretation models estimate rock elastic properties based on rock composition, but they often fail to account for rock fabric effects, which cannot be neglected in shales because of their intrinsically complex structure. This thesis develops a method to quantify several rock fabric parameters based on rock composition and sonic/density logs. Such parameters are: load-bearing matrix, rock constituent shapes, presence of anisotropic cracks or fractures, and heterogeneity. Sonic logs are used as reference to validate rock fabric parameters. Results, combined with elastic properties and rock composition, are used to identify suitable zones for drilling horizontal wells and depth intervals to initiate hydraulic fractures and to contain fracture propagation.

Other parameters may affect rock elastic properties but are not studied in this thesis. These include in-situ stress, pore pressure, and temperature. Herein we assume that rock elastic properties only vary with rock composition and rock fabric.

The method developed in this thesis invokes models with many variables. Assuming that rock composition is accurate (which is in itself a non-unique process), estimated parameters are rock fabric properties such as load-bearing solid phase, rock component shapes, and anisotropic inclusions and/or cracks. Only two outputs result from the estimation: compressional- and shear-wave velocities. Therefore, reproducing sonic logs with the method developed in this thesis may give rise to non-unique solutions. One should take into account geology, diagenesis, core data, and as much available external information as possible to secure reliable, accurate, and petrophysically viable results. One should also take into account that shale gas formations are usually unique in their behavior, hence models should be carefully extrapolated from one shale to another. Likewise, caution should be used to extrapolate a model from one well to another in a laterally heterogeneous formation.

1.2 PREVIOUS WORK

Many theories and methods have been developed to assess elastic properties of rocks from their composition, each having different assumptions and limitations. Empirical models, such as Wyllie's time-average equation (Wyllie et al., 1956, 1958), are useful for assessing velocities, from which elastic properties can be derived in isotropic and homogeneous rocks. Even though they provide fast and reliable estimations in many conventional reservoirs, these models neglect the intrinsic complexity of shales.

More complex theoretical models have been formulated to estimate elastic properties from mixtures of grains and pores, usually referred to as effective medium elastic theories, or mixing laws. Hashin and Shtrikman (1963) derived bounds for the value of bulk and shear moduli in isotropic rocks. Any estimation of elastic properties from mineralogy and porosity must fall within these bounds. Kuster and Toksöz (1974) developed a long-wavelength, first-order scattering theory to approximate compressional- and shear-wave velocities. A more general form of their theory can account for different inclusion shapes (Kuster and Toksöz, 1974; Berryman, 1980). Unless used with small portions of inclusions, this model can violate the Hashin-Shtrikman bounds. The self-consistent approximation (SCA) was developed to accommodate higher concentrations of inclusions (Budiansky, 1965; Hill, 1965; Wu, 1966). This effective medium theory describes the deformation of inclusions in a background medium of yet-to-be-known elastic properties. Whereas the SCA honors Hashin-Shtrikman bounds, a specific phase is topologically connected only over a narrow volumetric concentration range: 40 to 60% for spherical inclusions (Berryman, 1980). This becomes a limitation when the load-bearing phase accounts for less than 40% of the total rock composition. The differential effective medium theory was developed to quantify elastic properties of a rock in which a component is load-bearing. Originally derived by Bruggeman (1935), this model

incrementally adds inclusions in a host matrix that remains spatially connected even at low concentrations. Combinations of the self-consistent approximation and the differential effective medium have been used to model the elastic properties of rocks with two connected phases (Sheng, 1990, 1991).

Previously described effective medium theories assume isotropic rocks and do not account for presence of anisotropic cracks or inclusions. Horizontal compliant pores or vertical fractures, for example, are often encountered in shale formations and can affect elastic properties. Therefore, they should not be neglected in a rock physics model applied to an anisotropic shale formation. Hudson (1980) developed a model to estimate the effects of thin, penny-shaped (ellipsoidal) cracks in isotropic media. The model was extended to describe heavily faulted structures by Hudson and Liu (1999). Such theories are used to simulate anisotropic elastic properties due to the anisotropic distribution of inclusions, either solid or filled with fluids.

Another limitation of the previously described effective medium theories is that they assume high-frequency conditions if fluids are directly mixed with rock solid components. On the other hand, sonic logs—used to validate simulations—measure low-frequency velocities (from which elastic properties are derived). Gassmann's relation (Gassmann, 1951; Biot, 1956) estimates low-frequency elastic properties of saturated rocks, either isotropic or anisotropic.

Combinations of effective medium theories and fluid saturation models have been shown to describe reliably the elastic properties of complex formations, such as shales or tight gas, by accurately accounting for the combined effects of in-situ grain and pore shapes (Xu and White, 1995; Smith et al., 2009; Ruiz and Cheng., 2010).

1.3 OBJECTIVES

Assuming that rock composition is known and sonic/density logs are available, the first objective of this thesis is to identify and quantify several rock fabric parameters of hydrocarbon-bearing shale formations: load-bearing matrix, shape of rock components, presence of oriented cracks (compliant pores or fractures for example), and heterogeneity. Several rock physics models are invoked to estimate elastic properties of a rock with specific fabric attributes. Velocities are calculated from estimated elastic properties and compared to field data. Rock fabric is validated when simulations accurately reproduce sonic logs. Errors indicate erroneous simulation parameters, unexpected rock fabric at a certain location, or an incorrect model. To account for the complex structure of shales and accurately estimate rock elastic properties, the simulation/interpretation method must honor the following properties:

- Multi-minerals: shale gas usually exhibits a complex solid composition comprising various amounts of silica, carbonate material, kerogen, pyrite, ankerite, apatite, and others. Individual solid concentrations change with depth; it would be inaccurate to assume depth-constant elastic properties of the rock's solid framework.
- Load-bearing matrix: Hornby et al. (1994) describe how certain minerals in shales, usually clay, make up the skeleton of the rock by constituting a topologically connected load-bearing phase. This concept is particularly important for identifying suitable zones to drill a horizontal well. Layers with a brittle load-bearing matrix (made of silica or calcite, for example) are preferred over intervals with ductile load-bearing matrix (made of clay, for example) because they provide more resistance to collapse and embedment.

- Anisotropy: most gas-bearing shales are anisotropic (Vernik and Milovac, 2011). This behavior can be due to many factors, such as alignment of thin mineral particles (clay pellets or shells, for example), horizontal compliant pores that deformed under compaction stress, fractures, or both aligned mineral grains and pores. In an anisotropic formation, whenever isotropic simulation is shown to reproduce sonic logs reliably, it may indicate that rock fabric is not the main cause of anisotropy; it could be primarily due to stress, for example.
- Heterogeneity: similar to rock composition, rock fabric may be vertically variable. In the same formation, the load-bearing component or the density of fractures may change with depth, for example. If rock fabric components are shown to vary with depth, rock typing is invoked to divide the formation into groups of layers that exhibit similar properties. Each group is associated with a specific set of rock fabric parameters.
- Low-frequency: elastic properties calculated from sonic logs are usually regarded as low-frequency dynamic elastic properties. Unless combined with a fluid saturation model such as Gassmann's theory, effective medium theories estimate high-frequency dynamic elastic moduli. Such a simulation must be compared to ultrasonic core measurements for consistency. Therefore, the model must estimate low-frequency dynamic elastic properties whenever simulations are validated with sonic logs.

The second objective of this thesis is to interpret the quantified rock fabric properties to assess suitable zones for drilling horizontal wells and to initiate or contain hydraulic fracture propagation. Brittle load-bearing matrix, high Young's modulus—if available—, limited layering, and proximity to favorable production intervals are

properties that indicate suitable zones for drilling a horizontal well. Production intervals should exhibit sizeable amounts of gas and organic content. For optimal hydraulic fracturing they should also be brittle and non-laminated. Even though natural fractures could provide additional flow paths, they could also absorb hydraulic stimulation energy and become counter-productive; therefore, one should avoid intervals with high concentrations of natural fractures during such operations. Hydraulic stimulation should also be avoided in depth intervals exhibiting such fractures whenever they are connected to a water-bearing formation, because of the risk of water production. Suitable intervals for fracture containment are either very stiff (carbonate layers, for example, usually that do not rupture under fracture pressure) or very soft (clay-rich layers, for example, that absorb fracturing energy and heal/close fractures). They must also include no natural fractures (especially in stiff confining layers) so that fracturing fluids do not flow through these intervals.

1.4 Outline of the Thesis

Chapter 2 describes the rock physics models invoked to estimate elastic properties and velocities from rock composition and rock fabric. It also describes the rock typing approach used in vertically heterogeneous formations, as well as the averaging method implemented to consistently compare simulations to well logs. Chapter 3 documents several synthetic examples constructed to illustrate the impact of rock fabric on elastic properties, and velocities. Field studies from Haynesville and Barnett shales are introduced in Chapters 4 and 5, respectively. Chapter 6 summaries the conclusions and suggestions for future work. The Appendix provides details about the formulations of first-order correction coefficients for Hudson's model.

Chapter 2: Method

This chapter describes the workflow developed to estimate elastic properties and velocities in organic source rocks. It is based on rock composition and rock fabric. The inversion method used to estimate rock solid composition, porosity, fluid types, and fluid saturations is introduced first. Calculation of elastic properties from sonic and density logs is detailed in this chapter, as well as the calculation of velocities from stiffness tensors. Construction of rock skeleton and dry frame, addition of anisotropic cracks or inclusions, and saturation with fluids are described with their respective rock physics models. For strata exhibiting vertical heterogeneity, the formation is divided into rock types on the basis of rock composition. Specific rock fabric properties are identified and quantified for each rock type.

2.1 Inversion of Petrophysical Properties from Well Logs

Evaluation of petrophysical properties of hydrocarbon-bearing shales is difficult because of the complex composition and high spatial variability of shale properties. Shale is composed of numerous solid elements—such as quartz, calcite, clay, pyrite, and kerogen—often arranged in the form of thin layers whose size is smaller than the vertical resolution of conventional logging measurements (7 to 10 inches in average for most measurements). Figure 2.1 gives an example of the complex structure of a typical shale. This example, from the Barnett shale, is a laminated siliceous mudstone comprising clay, quartz, carbonate material, and other minerals in minor amounts. Magenta lines represent induced fractures, both parallel and perpendicular to bedding plane—horizontal in this example—. Heidari (2011) developed a deterministic nonlinear inversion method from conventional well logs that is amenable to the interpretation of hydrocarbon-bearing

shales. Heidari's method assumes conventional logs such as density, neutron porosity, photoelectric factor, and spectral gamma ray. Adiguna (2012) refined the method and proposed a practical workflow to estimate rock solid composition, porosity, fluid types, and fluid saturation. The method was successfully applied to data acquired in the Haynesville and Barnett shales. Results were validated by comparison to core measurements and neutron capture spectroscopy logs.

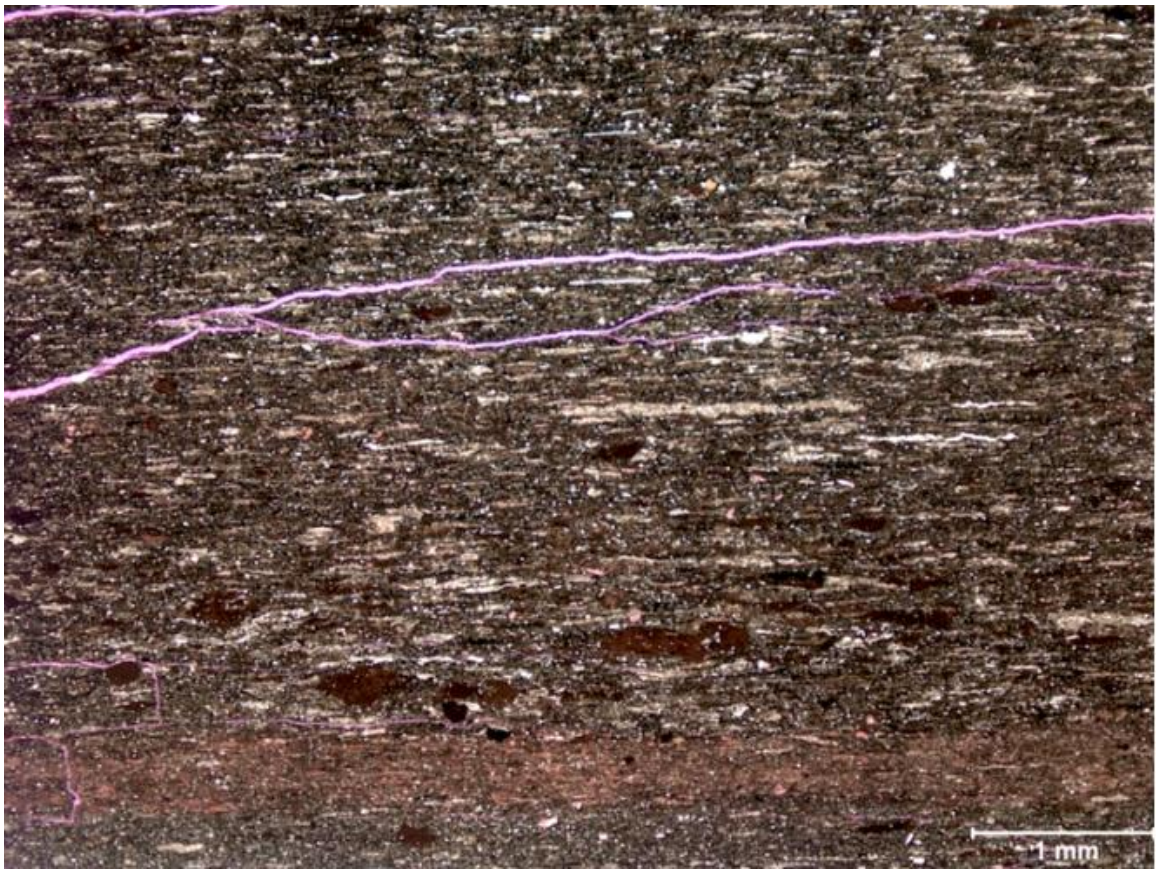

Figure 2.1: Thin section from the Barnett shale. Pink lines identify microfractures (the order of magnitude of fracture thickness in this example is ten micrometers). Main constituents in this rock are quartz, calcite, clay, and kerogen.

2.2 SONIC LOGS, ELASTIC MODULI, AND STIFFNESS TENSORS

This section explains how elastic properties are calculated from sonic and density logs and shows the differences between isotropic and transverse isotropic stiffness tensors.

Hooke's law describes the relation between stress and strain of a solid. Its general form for an anisotropic, linear, and elastic solid is given by

$$\sigma_{ij} = c_{ijkl}\varepsilon_{kl}, \tag{2.1}$$

where σ_{ij} is stress, ε_{kl} is strain, and c_{ijkl} is elastic stiffness tensor. The stiffness tensor can be expressed in the following matrix form using Voigt's notation:

$$c_{IJ} = \begin{bmatrix} c_{11} & c_{12} & c_{13} & c_{14} & c_{15} & c_{16} \\ c_{21} & c_{22} & c_{23} & c_{24} & c_{25} & c_{26} \\ c_{31} & c_{32} & c_{33} & c_{34} & c_{35} & c_{36} \\ c_{41} & c_{42} & c_{43} & c_{44} & c_{45} & c_{46} \\ c_{51} & c_{52} & c_{53} & c_{54} & c_{55} & c_{56} \\ c_{61} & c_{62} & c_{63} & c_{64} & c_{65} & c_{66} \end{bmatrix}, \tag{2.2}$$

where c_{IJ} represents c_{ijkl} in Voigt's notation and assuming the following indices transformation:

ij(kl)	*IJ*
11	*1*
22	*2*
33	*3*
23, 32	*4*
13, 31	*5*
12, 21	*6*

(2.3)

For an isotropic medium, the stiffness tensor contains only two independent entries and has the form

$$c_{IJ} = \begin{bmatrix} c_{11} & c_{12} & c_{12} & 0 & 0 & 0 \\ c_{12} & c_{11} & c_{12} & 0 & 0 & 0 \\ c_{12} & c_{12} & c_{11} & 0 & 0 & 0 \\ 0 & 0 & 0 & c_{44} & 0 & 0 \\ 0 & 0 & 0 & 0 & c_{44} & 0 \\ 0 & 0 & 0 & 0 & 0 & c_{44} \end{bmatrix}, \tag{2.4}$$

where $c_{12} = c_{11} - 2c_{44}$. For such media, one can define two independent elastic moduli: bulk modulus and shear modulus. Bulk modulus is given by

$$K = c_{11} - \frac{4}{3}c_{44}\,, \tag{2.5}$$

and shear modulus by

$$\mu = c_{44} . \tag{2.6}$$

From these two independent elastic moduli, one can calculate Young's modulus and Poisson's ratio. Young's modulus is given by

$$E = \frac{9K\mu}{3K + \mu} , \tag{2.7}$$

and Poisson's ratio is given by

$$\nu = \frac{3K - 2\mu}{2(3K + \mu)} . \tag{2.8}$$

In vertical transverse isotropic media, the stiffness tensor contains five independent entries and exhibits the form

$$c_{IJ} = \begin{bmatrix} c_{11} & c_{12} & c_{13} & 0 & 0 & 0 \\ c_{12} & c_{11} & c_{13} & 0 & 0 & 0 \\ c_{13} & c_{13} & c_{33} & 0 & 0 & 0 \\ 0 & 0 & 0 & c_{44} & 0 & 0 \\ 0 & 0 & 0 & 0 & c_{44} & 0 \\ 0 & 0 & 0 & 0 & 0 & c_{66} \end{bmatrix}, \tag{2.9}$$

where $c_{66} = ½(c_{11} - c_{12})$.

Velocities are functions of elastic properties and bulk density, ρ_b, of the rock. For isotropic formations, compressional- and shear-wave velocities, V_P and V_S, respectively, are calculated using the formulae

$$V_P = \sqrt{\frac{c_{11}}{\rho_b}} = \sqrt{\frac{K + \frac{4}{3}\mu}{\rho_b}} , \tag{2.10}$$

and

$$V_S = \sqrt{\frac{c_{44}}{\rho_b}} = \sqrt{\frac{\mu}{\rho_b}} . \tag{2.11}$$

For transverse isotropic media, where θ is the angle between the wave vector and the axis of symmetry of the rock, one distinguishes between one compressional- and two shear-wave velocities. Compressional velocity, also referred to as quasi-longitudinal mode, is given by

$$V_{P\_TI} = \left(c_{11}sin^2\theta + c_{33}cos^2\theta + c_{44} + \sqrt{M}\right)^{\frac{1}{2}} (2\rho_b)^{-1/2} , \tag{2.12}$$

quasi-shear velocity by

$$V_{QS\_TI} = \left(c_{11}sin^2\theta + c_{33}cos^2\theta + c_{44} - \sqrt{M}\right)^{\frac{1}{2}} (2\rho_b)^{-1/2} , \tag{2.13}$$

and pure shear velocity by

$$V_{PS\_TI} = \left(\frac{c_{66}sin^2\theta + c_{44}cos^2\theta}{\rho_b}\right)^{1/2} , \tag{2.14}$$

where

$$M = [(c_{11} - c_{44})sin^2\theta - (c_{33} - c_{44})cos^2\theta]^2 + (c_{13} + c_{44})^2 sin^2 2\theta \quad (2.15)$$

(Mavko et al., 2009).

2.3 ROCK PHYSICS MODELS

This section describes how several rock physics models are combined to construct a rock with specific fabric. The solid phase of the rock is the mixture of all its solid constituents, with no regard to their spatial arrangement or shape. The dry frame accounts for the spatial distribution of rock components, including load-bearing matrix, shape of solids and dry pores, and dry anisotropic cracks or inclusions. The saturated rock is the dry frame in which porous space is filled with mixtures of water and hydrocarbons.

2.3.1 Construction of the dry isotropic frame of the rock

Construction of the dry isotropic rock frame is the first step in estimating rock elastic properties. It involves choosing of a preferential load-bearing solid phase—which can be composed of either one or two minerals—and choice of shape of non-connected inclusions. A fraction of porosity is added and represents the isotropic portion of the pore space. For the rock physics models used in this thesis, the connected solid phase is considered as load-bearing (Hornby et al., 1994).

The selection of load-bearing phase is trivial in simple formations: in consolidated sandstones, for example, quartz grains are in contact with each other and support loads through the solid network they constitute. In horizontally laminated sequences constituted

of two types of layers, the two laminated solid phases support the vertical load. However, for mixtures of different minerals and organic content, as it is the case in organic shales, the concept of load-bearing matrix is more complex. There is not always a clear dominant mineral (in terms of volumetric concentration) in the rock framework.

We choose two isotropic rock physics models to construct the dry isotropic frame of the rock: the self-consistent approximation (SCA) and the differential effective medium (DEM) theory. Both these effective theories estimate bulk and shear moduli of a mixture of phases. Porous space must be dry—both elastic moduli are set to zero—and saturated subsequently in order to simulate low-frequency conditions. Inclusions are assumed to exhibit idealized ellipsoidal shapes. Media are assumed to be isotropic, linear and elastic.

Berryman (1980, 1995) develops a general formulation of the self-consistent approximation for a mixture of N phases, given by

$$\sum_{i=1}^{N} x_i \, (K_i - K_{SC}^*) \, P^{*i} = 0 \ , \tag{2.16}$$

and

$$\sum_{i=1}^{N} x_i \, (\mu_i - \mu_{SC}^*) \, Q^{*i} = 0 \ , \tag{2.17}$$

where i refers to the i-th material, x_i represents its volumetric concentration and P and Q are geometric coefficients. Superscripts $*i$ on P and Q indicate that the factors are for the i-th inclusion in a background medium with elastic moduli K^*_{SC} and μ^*_{SC}. Table 2.1

summaries P and Q formulae for two shapes: spheres and penny-shaped cracks. A penny-shaped crack is characterized by its aspect ratio, α, which is the ratio of short to long axes. An aspect ratio of 1 implies that the crack is a sphere whereas a value of 0 means that the crack is a disk of zero thickness. In the self-consistent approximation, no constituent is regarded as host material (and therefore load-bearing), except in specific cases discussed later. It estimates elastic properties of an aggregate of all rock constituents. For that reason, the self-consistent approximation is usually not suitable for estimating elastic properties of a rock in which a certain mineral, or combination of several minerals, is load-bearing (Hornby et al., 1994).

Inclusion Shape	P^{mi}	Q^{mi}
Sphere	$\frac{K_m + \frac{4}{3}\mu_m}{K_i + \frac{4}{3}\mu_m}$	$\frac{\mu_m + \zeta_m}{\mu_i + \zeta_m}$
Penny Crack	$\frac{K_m + \frac{4}{3}\mu_i}{K_i + \frac{4}{3}\mu_i + \pi\alpha_i\beta_m}$	$\frac{1}{5}[1 + \frac{8\mu_m}{4\mu_i + \pi\alpha_i(\mu_m + 2\beta_m)} + 2\frac{K_i + \frac{2}{3}(\mu_i + \mu_m)}{K_i + \frac{4}{3}\mu_i + \pi\alpha_i\beta_m}]$

Notes:

$$\beta_m = \mu\frac{(3K_m + \mu_m)}{(3K_m + 4\mu_m)}$$

$$\zeta_m = \frac{\mu_m}{6}\frac{(9K_m + 8\mu_m)}{(K_m + 2\mu_m)}$$

Table 2.1: *P* and *Q* coefficients used in the self-consistent approximation for spherical and ellipsoidal (penny crack) shapes. *K*, μ are bulk and shear moduli, respectively. α is the penny crack aspect ratio. Subscripts *m* and *i* designate the background and inclusion material, respectively (Berryman, 1980; Mavko et al., 2009).

The differential effective medium theory estimates bulk and shear moduli of a two-phase mixture. Phase 1 is the host; it remains topologically connected regardless of concentration. Phase 2 is incrementally added to the host material until it reaches its

desired concentration, x_2. Berryman (1992) gives the following formulation for the DEM differential equations:

$$(1-x)\frac{\partial}{\partial x}[K^*(x)] = (K_2 - K^*_{DEM})P^{*2}(x)\,, \tag{2.18}$$

and

$$(1-x)\frac{\partial}{\partial x}[\mu^*(x)] = (\mu_2 - \mu^*_{DEM})Q^{*2}(x)\,, \tag{2.19}$$

with initial conditions $K^*(x=0) = K_1$ and $\mu^*(x=0) = \mu_1$, where subscripts or superscripts *1* and *2* refer to host and inclusion materials, respectively; K^*_{DEM} and μ^*_{DEM} are the bulk and shear moduli of the mixture, respectively. Geometric factors *P* and *Q* are identical to those of the self-consistent approximation, and superscript *2 indicate that coefficients *P* and *Q* are for an inclusion of material 2 in a background medium with bulk and shear moduli K^*_{DEM} and u^*_{DEM}, respectively. Their formulations are given in Table 2.1. If there is more than one secondary phase, one calculates the mixture's effective elastic properties in several steps, adding one type of inclusion after another. The order in which inclusions are added does not necessarily reflect the true geological evolution of the rock (Mavko et al., 2009).

Independently, neither the self-consistent approximation nor the differential effective medium theory are reliable to describe the behavior of rocks that exhibit several topologically connected phases. Hornby et al. (1994) describe how combining the self-consistent approximation and the differential effective medium theory provides a solution to this problem. If two materials of concentration between 40 and 60% are mixed using the self-consistent approximation and assuming spherical shapes, the two phases are

connected within the mixture. The differential effective medium model is subsequently invoked to adjust relative concentrations of the two materials. This combination of the SCA and the DEM allows one to model rocks that exhibit two load-bearing components.

Using the differential effective medium theory, or a combination of the differential effective medium theory and the self-consistent approximation, one can estimate elastic properties of different mixtures of minerals. Simulation parameters include load-bearing phase—composed of one or two solids—, order in which inclusions are added, and shape of inclusions.

2.3.2 Treatment of anisotropic cracks and inclusions

In this section, and subsequently when referring to anisotropic simulations, anisotropic inclusions refer to oriented solid rock components and anisotropic cracks refer to oriented pores.

Hudson's model (1980) is based on a scattering theory and describes the effect of oriented ellipsoidal inclusions or cracks in an isotropic background medium on rock elastic properties. Before constructing the rock isotropic matrix, one chooses a percentage of certain minerals and a percentage of porosity to be modeled as oriented inclusions or cracks. Elastic moduli of cracks (oriented pores) are set to zero and the rock is subsequently saturated with fluids in order to honor low-frequency conditions.

Hudson's model estimates effective moduli of rocks that contain oriented penny cracks, or inclusions, by adding first- and second-order corrections to the entries of the isotropic background stiffness tensor, namely,

$$c_{IJ}^{eff} = c_{IJ}^{0} + c_{IJ}^{1} + c_{IJ}^{2}, \tag{2.20}$$

where superscripts *0*, *1*, and *2* identify background, first-order correction, and second-order correction, respectively. We use only first-order correction because the second-order correction can lead to convergence problems (Cheng, 1993). The Appendix details the formulation of first-order correction terms.

It is important to ensure that crack density, ε_{crack}, remains under the limiting value of 0.1 given by Hudson (Mavko et al., 2009). Crack density depends on concentration of cracks or inclusions, and their aspect ratio; it is given by

$$\varepsilon_{crack} = \frac{3x_{crack}}{4\pi\alpha_{crack}}, \tag{2.21}$$

where x_{crack} and α_{crack} are the volumetric concentration of cracks—or inclusions—and their aspect ratio, respectively.

2.3.3 Treatment of fluid saturation

After adding oriented cracks and inclusions to the isotropic matrix, one must take into account the effect of fluids that fill the porous space. In the field studies described in this thesis, hydrocarbons are gas. Therefore, pore space is assumed to contain only two fluids: water and gas. The Bulk modulus of the fluid mixture is estimated with Reuss's formula (Reuss, 1929):

$$K_{flu} = \left[\frac{s_w}{K_w} + \frac{(1 - s_w)}{K_g}\right]^{-1} \tag{2.22}$$

where K_w and K_g are the bulk modulus of water and gas, respectively; s_w is saturation of water. The shear modulus of the fluid mixture is zero.

In isotropic media, rocks are saturated using the isotropic formulation of Gassmann's theory (Gassmann, 1951):

$$K_{sat} = K_{dry} + \frac{(1 - K_{dry}/K_0)^2}{\frac{\Phi}{K_{flu}} + \frac{1-\Phi}{K_0} - \frac{K_{dry}}{K_0^2}}, \tag{2.23}$$

where K_{sat}, K_{dry}, K_0, and K_{flu} are bulk modulus of the saturated rock, bulk modulus of the dry frame, bulk modulus of the solid phase, and bulk modulus of the fluid mixture, respectively; Φ is total porosity of the rock, and K_0 is assumed to be equal to the previously estimated bulk modulus of the isotropic solid mixture. Pore-pressures are assumed to be equilibrated in the pore space to honor low-frequency conditions. The rock is also assumed to be fully saturated with fluids.

Gassmann (1951) also provides a fluid-substitution formulation for the case of anisotropic rocks. Entries of the stiffness tensor for the saturated rock are given by

$$c_{ijkl}^{sat} = c_{ijkl}^{dry} + \frac{(K_0\delta_{ij} - \frac{c_{ijaa}^{dry}}{3})(K_0\delta_{kl} - \frac{c_{bbkl}^{dry}}{3})}{\left(\frac{K_0}{K_{flu}}\right)\phi\left(K_0 - K_{flu}\right) + (K_0 - \frac{c_{ccdd}^{dry}}{9})}, \tag{2.24}$$

where c_{ijkl}^{dry}, K_0, and K_{flu} are elastic stiffness tensor entries for the dry rock, bulk modulus of the isotropic solid mixture, and bulk modulus of the fluid mixture, respectively; Φ is total porosity of the rock, and K_0 is calculated in a similar way to the isotropic

formulation of Gassmann's theory: the entire solid mixture is modeled as isotropic using identical inclusion order and aspect ratios. In equation 2.24, a repeated index indicates a sum from 1 to 3 (for example, $c_{ijaa} = c_{ij11} + c_{ij22} + c_{ij33}$). Porosity is not included in the calculation of K_0; δ_{ij} is given by

$$\delta_{ij} = \begin{cases} 1 & for\ i = j \\ 0 & for\ i \neq j \end{cases}$$

2.4 ROCK TYPING

Using identical rock fabric along the entire depth interval of a formation can give good estimations of elastic properties and velocities. However, one may have to divide the formation into segments of similar properties that are subsequently associated with specific rock fabric properties. In the Barnett field wells, for instance, several rock types are identified (five for Well B1 and three for Well B2), and a specific rock fabric is associated with each rock type. Such a procedure suggests that rock fabric is vertically heterogeneous, which is commonly observed in shale formations. Rock typing in this thesis is based on solid volumetric composition of the formation, more specifically on volumetric concentration of kerogen, quartz, and calcite. Specific rock fabric properties for each rock type are: load-bearing material (composed of one or two solid components), order in which other components are added to the background matrix, and aspect ratio of non-spherical inclusions (either solid or porous).

2.5 SPATIAL AVERAGING OF ELASTIC PROPERTIES

Sonic tools are composed of sources and an array of receivers. In field examples in this thesis, the array contains 13 receivers spaced at 0.5 ft intervals. Therefore,

velocities and elastic properties calculated from sonic/density logs represent averaged in-situ rock properties. Simulated elastic properties—estimated every 0.5 ft—must be vertically averaged so that velocities are consistently compared to sonic logs. Layers are assumed to be horizontal.

For anisotropic formations, vertical effective bulk and shear moduli of individual layers are given by

$$K^{eq\_V} = \rho_b V_{PV}^2 - \frac{4}{3}\rho_b V_{SV}^2 , \tag{2.25}$$

and

$$\mu^{eq\_V} = \rho_b V_{SV}^2 , \tag{2.26}$$

respectively. For isotropic layers, the effective vertical bulk and shear moduli are equal to the isotropic bulk and shear moduli, respectively.

All beds exhibit equal thickness and effective vertical elastic moduli are averaged with Backus' formula (Backus, 1962). Averaged effective vertical bulk modulus is given by

$$K^{ave\_V} = \left[\frac{1}{N_L}\sum_{l=1}^{N_L}\frac{1}{K_l^{eq\_V}}\right]^{-1} , \tag{2.27}$$

and averaged effective shear modulus by

$$\mu^{ave\_V} = \left[\frac{1}{N_L} \sum_{l=1}^{N_L} \frac{1}{\mu_l^{eq\_V}} \right]^{-1}, \tag{2.28}$$

where $K_l^{eq\_V}$ and $\mu_l^{eq\_V}$ are effective vertical bulk and shear moduli of the l-th layer, respectively, and N_L is number of averaged layers. All layers are assumed to be linearly elastic. It is assumed that there are no sources of intrinsic energy dissipation and layers thickness is much smaller than the acoustic wavelength.

To compute velocities from elastic moduli, one must also average rock bulk density. The following formula is used to calculate rock average density:

$$\rho^{ave\_V} = \left(\sum_{l=1}^{N_L} \rho_l \right) / N_L , \tag{2.29}$$

where ρ_l is density of the l-th bed and N_L is number of averaged layers.

Vertical compressional- and shear-wave velocities are calculated using the formulae

$$V_{PV\_ave} = \sqrt{\frac{K^{ave\_V} + \frac{4}{3}\mu^{ave\_V}}{\rho^{ave\_V}}}, \tag{2.30}$$

and,

$$V_{SV\_ave} = \sqrt{\frac{\mu^{ave\_V}}{\rho^{ave\_V}}} . \tag{2.31}$$

2.6 ELASTIC PROPERTIES OF INDIVIDUAL ROCK COMPONENTS

Table 2.2 describes the assumed elastic moduli and density of individual rock components. Clay is assumed to simultaneously account for the mixture of clay minerals and clay-bound water.

	Bulk Modulus K (GPa)	**Shear Modulus μ (GPa)**	**Density ρ (g/cm^3)**
Quartz[1]	36.6	45	2.65
Calcite[1]	76.8	32	2.71
Clay[1]	21	7	2.6
Kerogen[2]	8	4	1.3
Water	2.25	0	1.1
Gas	0.21	0	0.12

[1] Mavko et al. (2009)

[2] Ahmadov et al. (2009)

Table 2.2: Summary of elastic properties and density of rock components assumed in the estimation of rock elastic properties in synthetic and field cases.

Chapter 3: Synthetic Cases

Elastic properties and velocities are assumed to depend on rock composition and fabric. Assuming that rock solid composition, porosity, and fluid saturations are known, several rock fabric properties are quantified with the method developed in this thesis. Such fabric parameters are inputs to the rock physics models introduced in Chapter 2 and, in order to accurately reproduce sonic logs, one must quantify the effects of fabric on rock mechanical behavior. This chapter describes how load-bearing matrix, inclusion order, and anisotropic cracks or inclusions perturb rock elastic properties. It also discusses the averaging effect of measurements acquired across thin beds.

3.1 Host Material in the DEM

The first synthetic case describes variations of elastic properties in a synthetic porous rock with variation of the load-bearing matrix composition. Identifying which solid phase supports the load in a formation is valuable for assessing suitable zones to drill horizontal wells or to initiate hydraulic fractures.

Figure 3.1 shows the effects of two different hosting materials on rock elastic properties when the differential effective medium (DEM) theory is invoked in the simulations. The solid part of the synthetic rock is composed of 75% quartz and 25% clay. Porosity (dry) varies from 0% to 25%. The simulation is first performed using quartz as host, and then clay as host.

Within the entire range of porosity, the bulk and shear modulus values are larger when the load is supported by quartz, which exhibit larger elastic moduli than clay. Consequently, underestimated or overestimated formation stiffness may be caused by a wrong choice of the load-matrix composition in the simulations.

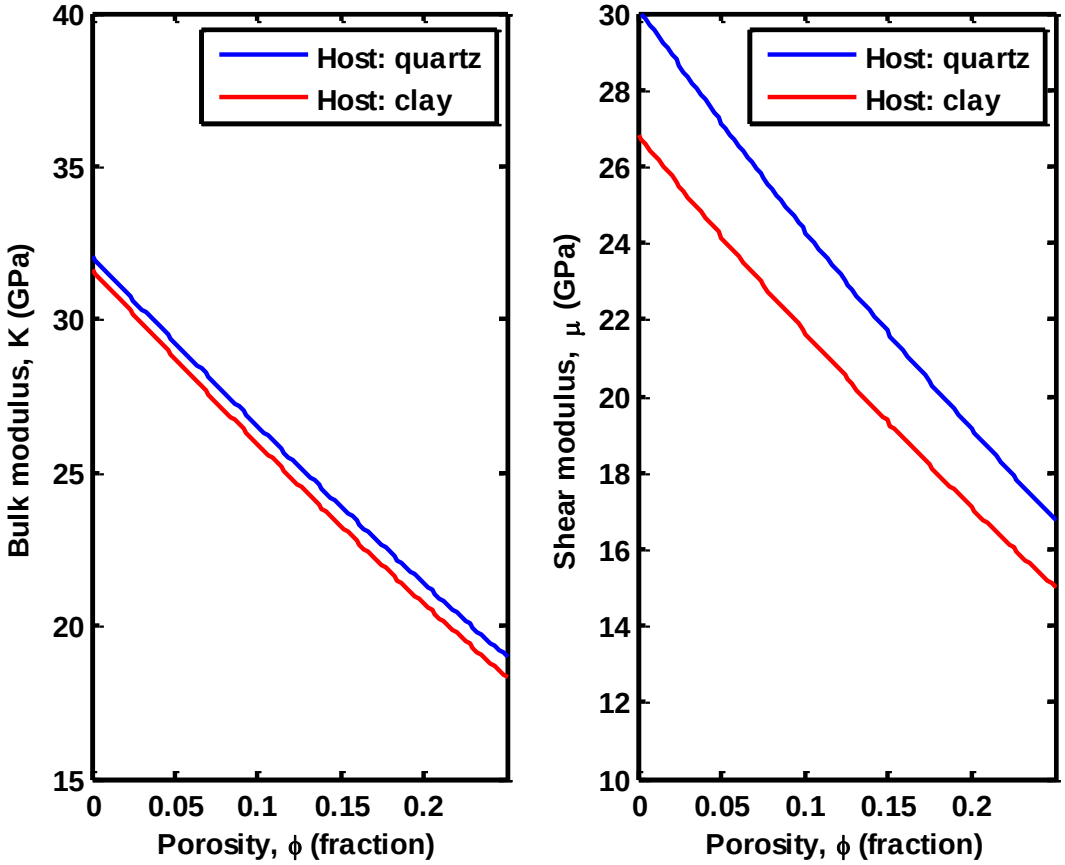

Figure 3.1: Variation of bulk modulus (left) and shear modulus (right) with porosity. The solid part of the rock is composed of 75% quartz and 25% clay. Blue and red curves identify cases where quartz and clay, respectively, are assumed to be the host component.

3.2 Inclusion Order in the DEM

The differential effective medium theory is invoked to model elastic properties of rocks that exhibit a topologically connected solid phase. This rock physics model estimates bulk and shear moduli of a two-phase mixture. In order to apply this model to cases where rock comprises more than two constituents, one adds one type of inclusion

after another. The effect of inclusion order on estimated rock elastic properties must be understood to follow reliable rock-physics workflows.

Figure 3.2 describes elastic properties of a synthetic rock in which the hosting material is quartz and inclusions of clay and calcite are added in different orders. The solid part of the synthetic rock is composed of 33% quartz, 33% clay, and 33% calcite. Dry porosity varies from 0% to 25%. In one example, clay is added first to quartz and then calcite is added to the mixture of quartz and clay. In the next examples, calcite is added first and clay second.

Calcite is the stiffest inclusion in this example, and the case where it is added prior to clay exhibits higher elastic moduli than in the case where clay is added first. Estimated formation stiffness is increased when stiff rock constituents are added before compliant inclusions, and decreased when compliant rock constituents are added first. Even though inclusion order must be taken into account in the simulations, this parameter usually has a lower effect on estimated rock elastic properties than load-bearing matrix composition. Therefore, load-bearing matrix is assessed first, and inclusion order is subsequently adjusted—if needed—to accurately reproduce sonic logs. Relative effects of different types of inclusion on rock elastic properties are inferred from inclusion order. For instance, in the case where calcite is added first and clay second, the DEM models a rock in which calcite inclusions are embedded into quartz and clay inclusions are embedded into the quartz-calcite mixture; in this example one can assume that calcite has more mechanical influence on the rock than clay because it partially hosts—together with quartz—the clay minerals.

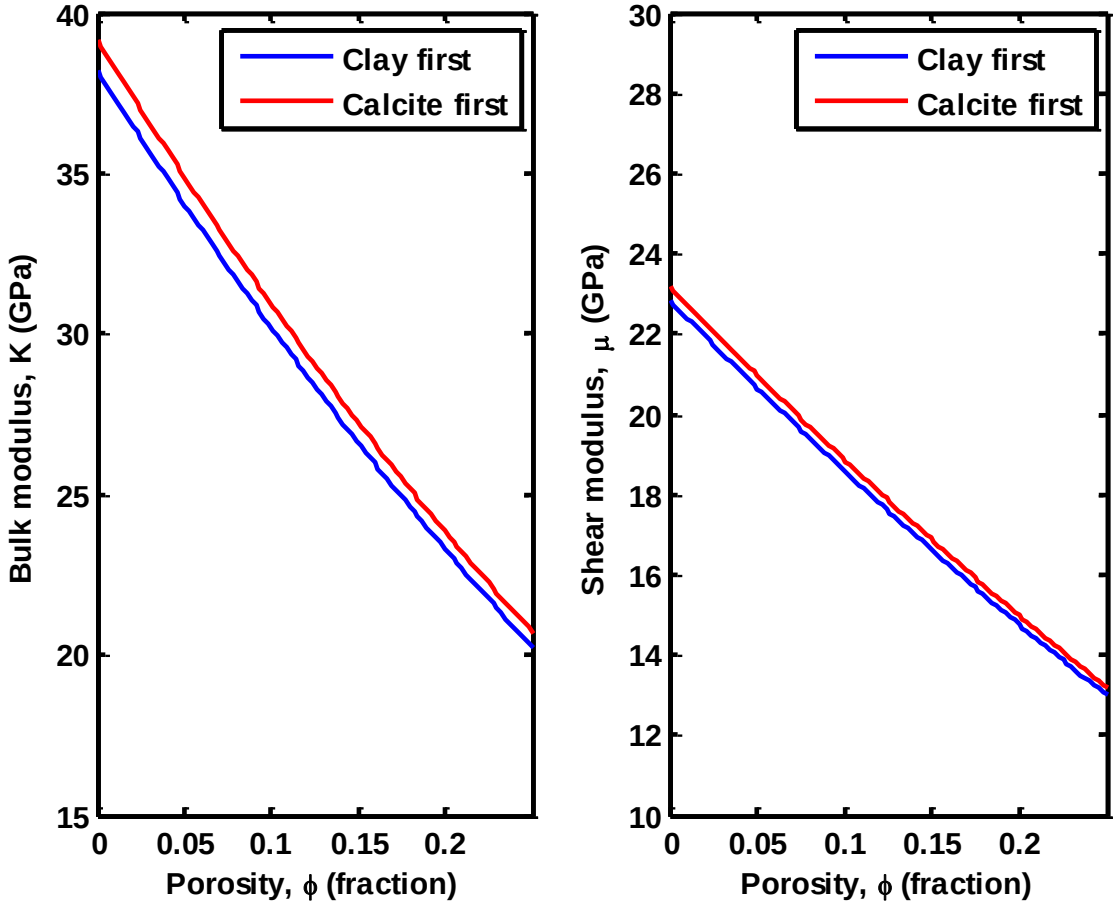

Figure 3.2: Variation of bulk modulus (left) and shear modulus (right) with porosity. The solid part of the rock is composed of 33% quartz, 33% clay, and 33% calcite. Quartz is the host material. Blue and red curves identify cases where clay is added first followed by calcite, and calcite is added first followed by clay, respectively.

3.3 HUDSON'S MODEL

Hudson's model is invoked to simulate the effect on rock elastic properties of anisotropic cracks or inclusions (such as natural fractures or horizontal compliant pores, for example) in an isotropic background. The third synthetic case is intended to study how velocities behave when specific rock constituents are assumed to exhibit an anisotropic distribution.

Figure 3.3 describes an application of Hudson's model to a synthetic rock. The synthetic rock is composed of 35% quartz, 20% calcite, 35% clay, and 10% dry porosity. In one example, a fraction of the porosity is modeled as horizontal cracks. In the other example, a fraction of calcite is modeled as horizontal inclusions. The isotropic part of the rock is modeled using the differential effective medium theory assuming spherical inclusions. Host material is clay. Quartz is added first, followed by calcite (the fraction that is not anisotropic), and then porosity (the fraction that is not anisotropic). Pore space, either isotropic or anisotropic, is dry, which means that the elastic moduli of pores are set to zero. Vertical shear velocity and horizontal quasi-shear velocity are equal (Mavko et al., 2009). Table 3.1 describes the maximum relative variation of velocities between isotropic and anisotropic media.

Simulation results indicate that modeling a fraction of pores as oriented cracks has more effect on velocities than modeling a fraction of a solid constituent as oriented stiff inclusions. In the case where a fraction of the porosity is assumed to be horizontally oriented, the vertical compressional-wave velocity varies approximately 3 times more than the horizontal compressional-wave velocity, whereas the vertical shear-wave velocity varies approximately 4 times less than the horizontal pure shear-wave velocity. Same relative behavior is observed in the case of stiff oriented inclusions, but with smaller variations in velocities. Vertical compressional- and horizontal shear-wave

velocities are more affected by horizontal orientation of rock constituents than horizontal compressional- and vertical shear-wave velocities, respectively. Such specific behaviors of compressional- and shear-wave velocities are used to quantify rock matrix anisotropy in the field examples.

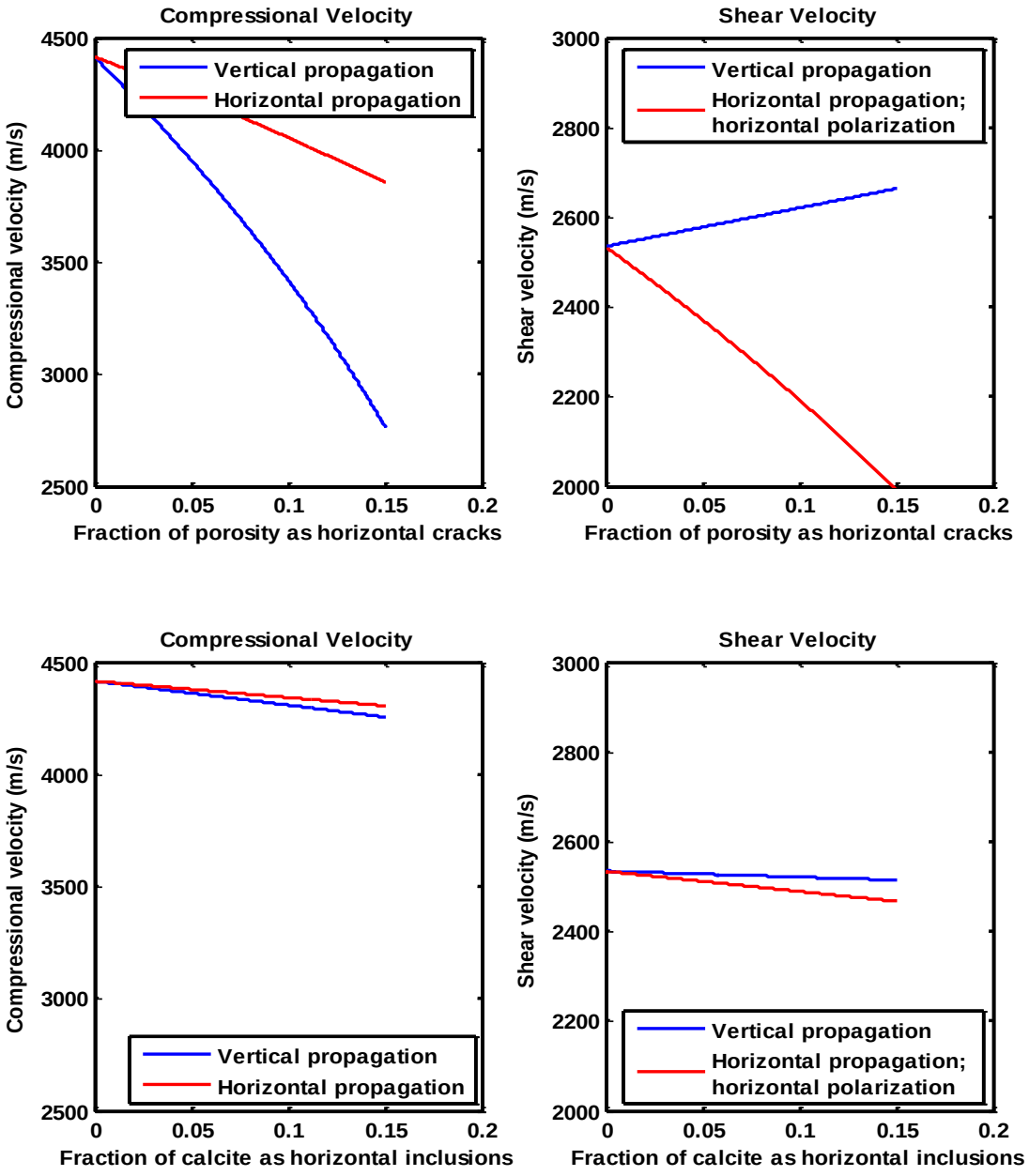

Figure 3.3: Synthetic case for Hudson's model. The rock is composed of 35% quartz, 20% calcite, 35% clay, and 10% dry porosity. Top two figures describe the case where a fraction of porosity is modeled as horizontal cracks of aspect ratio 0.1. Bottom two figures describe the case where a fraction of calcite is modeled as horizontal inclusions of aspect ratio 0.1. Left and right figures describe compressional and shear velocities, respectively. Blue and red curves identify vertical and horizontal direction of propagation, respectively.

	Compressional Velocity		Shear Velocity	
	Vertical propagation	Horizontal propagation	Vertical propagation	Horizontal propagation
(1) 15% of porosity modeled as horizontal cracks, compared to isotropic case	37.4%	12.7%	5.08%	21.3%
(2) 15% of calcite modeled as horizontal inclusions, compared to isotropic case	3.64%	2.51%	0.80%	2.67%

Table 3.1: Relative variation of velocities when (1) 15% of porosity is modeled as horizontal cracks of aspect ratio 0.1; (2) 15% of calcite is modeled as horizontal inclusions of aspect ratio 0.1. References for both velocities are isotropic values, where the fraction of horizontal cracks or inclusions is zero.

3.4 SPATIAL AVERAGING OF PROPERTIES

Simulated velocities are compared with sonic logs to validate rock fabric. In the field examples described in this thesis, elastic properties and velocities are estimated every 0.5 ft whereas sonic logs average formation properties over a larger interval (up to 6 ft). Therefore, in order to consistently compare estimations and field data, one must

average estimated elastic properties and velocities over a depth interval which thickness is equivalent to the length of the array of receivers of the sonic tool that was run in the well of interest.

Figure 3.4 describes a synthetic example of elastic properties and density with vertical Backus averaging. Two types of beds are assumed in the simulations:

- Sand layers: composed of 80% quartz and 20% water-filled porosity. Beds are 10 ft thick.
- Shale layers: composed of 30% quartz, 65% clay, and 5% water-filled porosity. Beds exhibit variable thicknesses: 10 ft, 5 ft, 2 ft, 1 ft, and 0.5 ft, from top to bottom.

The first and last beds (at the top and bottom, respectively) are sand. In this synthetic case, all beds are assumed to be isotropic. Table 3.2 describes assumed non-averaged values of elastic moduli and density for the two types of layers.

	Sand layers	**Shale layers**
Bulk Modulus K (GPa)	26.4	22.3
Shear Modulus μ (GPa)	28.2	10.7
Density ρ (g/cm^3)	2.34	2.61

Table 3.2: Summary of elastic moduli and density for sand and shale layers assumed in synthetic example 3.4 to discuss spatial averaging of properties.

In the case where both types of layers are thick—10 ft for example—, the averaging effect is only present at the interface between beds. As the thickness of one

type of bed decreases (less than 10 ft for the 6-feet average and less than 5 ft for the 3-feet average), elastic moduli and velocities do not reach their non-averaged values in the thin beds. If a formation exhibits thin beds, one can infer that acoustic logging measurements may not describe the true rock properties of these layers. Therefore, comparing non-averaged estimated velocities with field data is inaccurate and could result in erroneous conclusions.

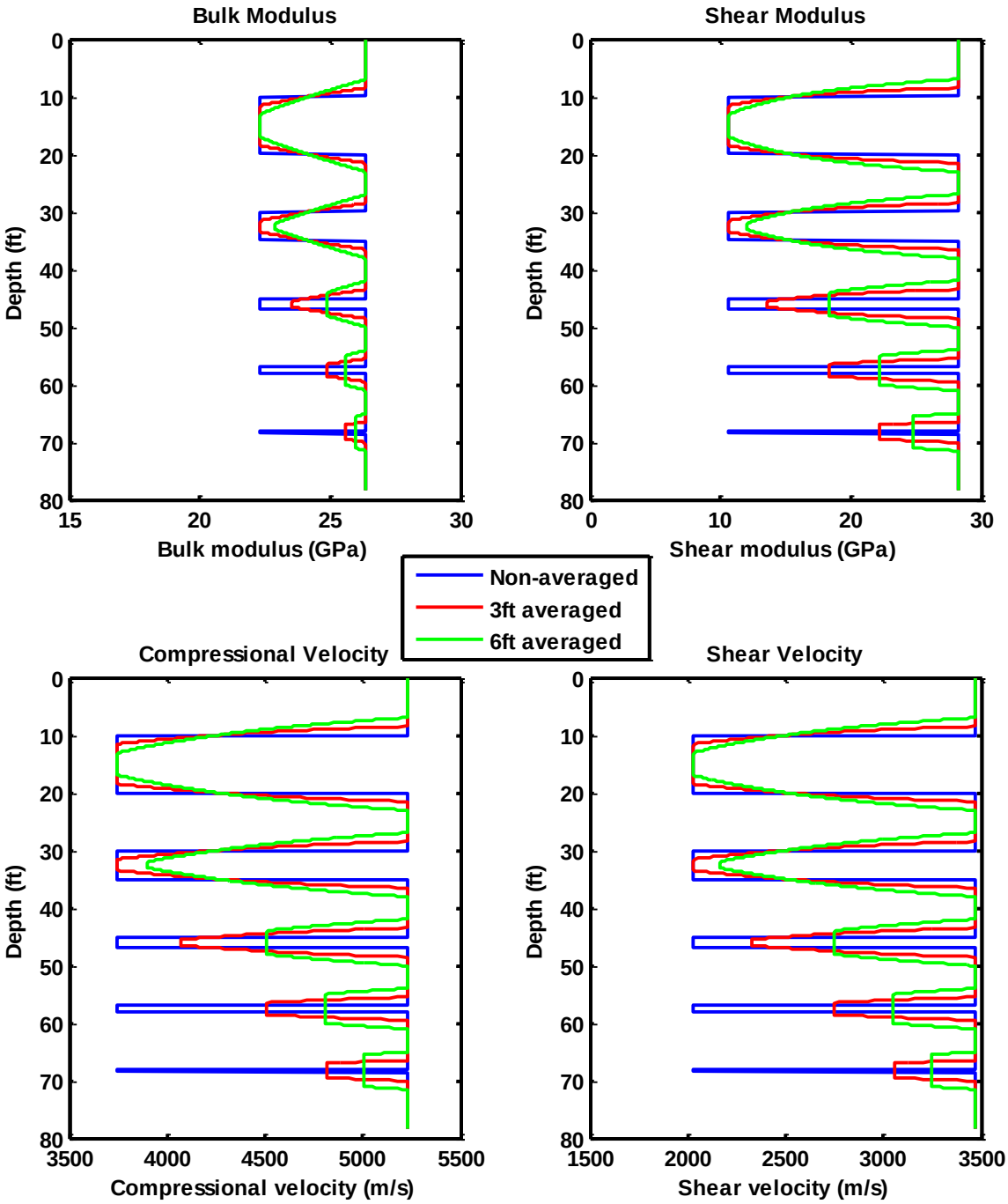

Figure 3.4: Synthetic example constructed to show the effect of thin beds on averaged elastic properties and velocities. Sand layers have a constant thickness of 10 ft. Shale layers have a decreasing thickness from top to bottom: 10 ft, 5 ft, 2 ft, 1 ft, and 0.5 ft.

Chapter 4: Haynesville Shale Case Study

This chapter describes the application of the previously described simulation and interpretation method in the Haynesville shale formation, a major shale gas field in the United States. Horizontal drilling and hydraulic fracturing are required for economically viable production of hydrocarbons. The purpose of this chapter is to quantify rock fabric properties in two wells and use the results to identify suitable zones for drilling horizontal wells and intervals to initiate or contain hydraulic fractures.

4.1 Background of the Haynesville Shale

The Haynesville shale is a major gas play in the United States. It is located in east Texas and northwest Louisiana, and has been long known to contain natural gas, but was only appraised as source rock because of its low permeability. Development of horizontal drilling and hydraulic fracturing enabled the production from organic-rich intervals. Haynesville shale is a black, organic-rich shale (Hammes et al., 2011). Its deposition occurred during Late Jurassic, about 150 million years ago. It is bounded by the Bossier shale above, and the Haynesville limestone and Smackover formation below (Hammes et al., 2011). Bossier shale is a silica-rich mudstone that exhibits large volumetric concentration of clay. Similar to the Smackover formation, the Haynesville limestone is primarily limestone, but it exhibits a larger clay content.

Conventional well logs are available in both wells and are used to estimate rock solid composition, porosity, fluid types, and fluid saturation. Compressional and shear velocity logs are available and describe vertical acoustic-wave properties—both wells were drilled in the vertical direction—. In the first example, velocities are simulated based on rock composition and fabric. They are compared to sonic logs in order to

validate fabric properties such as load-bearing matrix, inclusion order, anisotropy, and vertical heterogeneity. Once sonic logs are accurately reproduced, a similar model is invoked in the second well; the objective of extrapolating the rock physics model from one example to the other is to study lateral continuity of this region of the Haynesville shale. Simulation results are used to assess suitable zones for drilling horizontal wells and favorable intervals to initiate or contain hydraulic fractures.

Figure 4.1 shows the main logs acquired in Well H1. The transition from Bossier shale to Haynesville shale is inferred from a change in the neutron and density separation (black arrow 1) whereas the transition from Haynesville shale to Haynesville limestone is inferred from decrease of gamma-ray log due lower clay content (black arrow 2). The Smackover formation is below the Haynesville limestone, where gamma-ray values are low and become flat (black arrow 3).

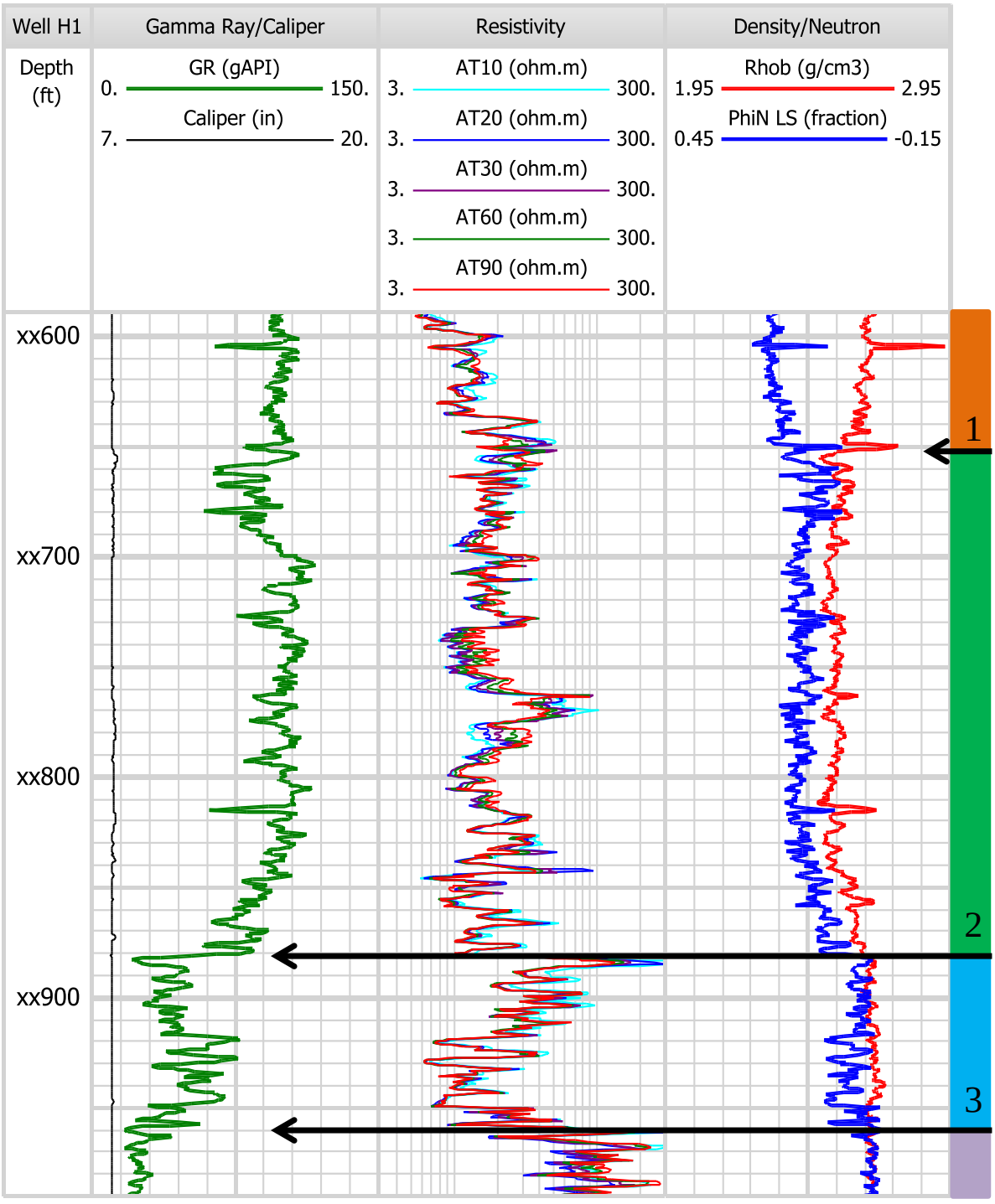
Well H1
Gamma Ray/Caliper
Resistivity
Density/Neutron
Depth (ft)
GR (gAPI)
0.
150.
Caliper (in)
7.
20.
AT10 (ohm.m)
3.
300.
AT20 (ohm.m)
3.
300.
AT30 (ohm.m)
3.
300.
AT60 (ohm.m)
3.
300.
AT90 (ohm.m)
3.
300.
Rhob (g/cm3)
1.95
2.95
PhiN LS (fraction)
0.45
-0.15
xx600
xx700
xx800
xx900
1
2
3

Figure 4.1: Main logs in Well H1. Track 1: relative depth. Track 2: gamma-ray and caliper logs. Track 3: apparent resistivity logs. Track 4: bulk density and neutron porosity (in limestone units) logs. Black arrows indicate transition from one formation to another: arrow 1 identifies transition from Bossier shale to Haynesville shale; arrow 2 identifies transition from Haynesville shale to Haynesville Limestone; arrow 3 identifies transition from Haynesville limestone to Smackover formation. Rectangles to the right indicate formation depth interval: orange for Bossier shale, green for Haynesville shale, blue for Haynesville limestone, and purple for Smackover limestone.

4.2 WELL H1

This section describes the application of the rock physics simulation and interpretation method in Well H1. Based on rock composition and fabric, compressional- and shear-wave velocities are simulated with an isotropic rock physics model. Load-bearing matrix, inclusion order, and vertical heterogeneity are quantified in the simulations. Rock fabric properties are validated when simulation accurately reproduce sonic logs. Results are discussed and used to assess suitable zones for drilling a horizontal well and to initiate or contain hydraulic fractures.

4.2.1 Mineralogy and rock physics model

Figure 4.2 shows the estimations of rock solid composition, porosity, and fluid saturations in Well H1. The interval of study, from xx650 ft to xx880 ft, corresponds to Haynesville shale depth interval with part of the transition to Haynesville limestone at the bottom. Additional minerals (such as pyrite and ankerite) may be present in small amounts, but only main constituents (quartz, calcite, clay, and kerogen) are used in the simulations. Well H1 exhibits stable amounts of kerogen above xx800 ft and higher vertical variability below this depth. Clay volumetric concentration is large (mean value

is equal to 37%), except from xx660 ft to xx690 ft and below xx860 ft, where volumetric concentrations of carbonate material are larger (mean values are equal to 31% and 38%, respectively; average volumetric concentration of calcite in the entire depth interval is equal to 17%). Formation exhibits carbonate streaks between xx690 ft and xx820 ft. Quartz volumetric concentration tends to correlate with clay content, decreasing as carbonate volumetric concentration increases.

Figure 4.3 describes the isotropic model that yields the best agreement with measured velocities. Rock fabric is constant throughout the entire simulation interval. The load-bearing matrix is assumed to be composed of clay and kerogen. Therefore, the first step is to invoke the SCA and DEM combination to model a background load-bearing matrix that comprises clay and organic matter. Though calcite exhibits a smaller volumetric concentration than quartz at most depths, carbonate inclusions are added first to the background matrix. All solids are modeled as spheres. Porosity is included last, assuming an ellipsoidal shape of aspect ratio 0.07. The rock is saturated using the isotropic formulation of Gassmann's theory.

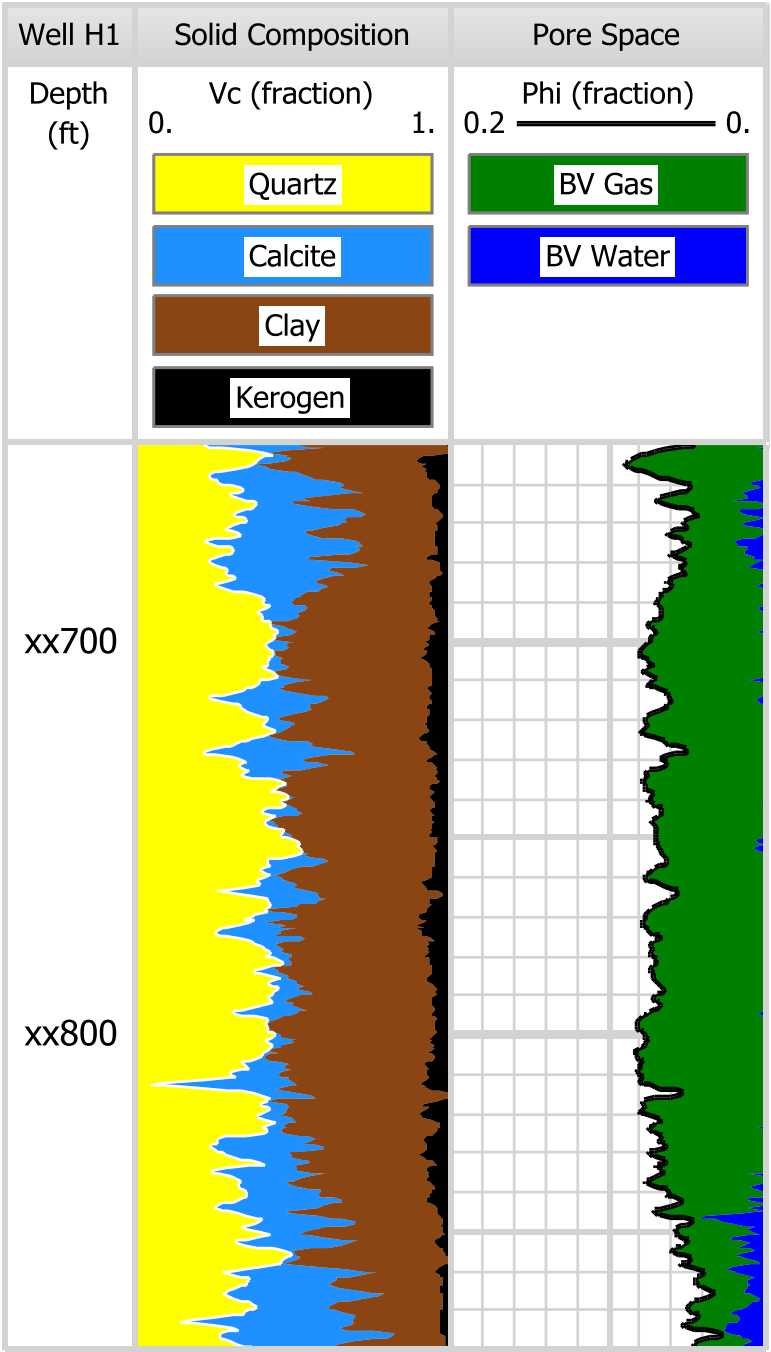

Figure 4.2: Rock composition in Well H1. Track 1: relative depth. Track 2: volumetric composition (Vc) of the solid part of the rock. Track 3: porosity and bulk volume (BV) of water and gas.

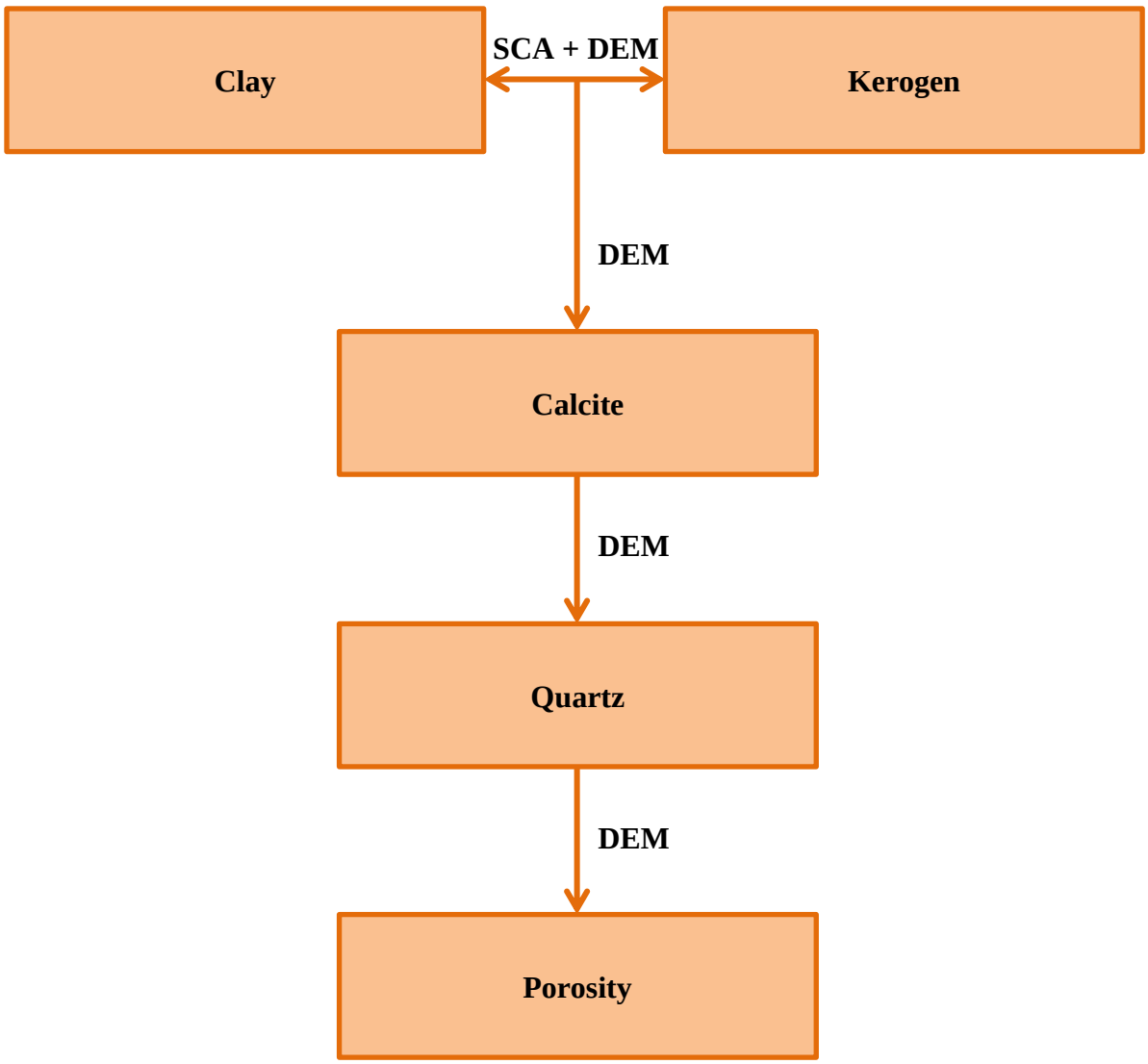

Figure 4.3: Rock physics model assumed in Well H1. The rock is saturated using the isotropic formulation of Gassmann's theory after porosity is added to the solid phase. SCA, DEM, and SCA + DEM designate the self-consistent approximation, the differential effective medium theory, and their combination (to model a rock that exhibits two load-bearing phases), respectively.

4.2.2 Simulation results

Figure 4.4 describes the results obtained from velocity estimations, showing both non-averaged and spatially averaged estimations. Spatially averaged estimated velocities are relevant when compared to sonic logs because sonic measurements implicitly average rock elastic properties and density. Table 4.1 describes the mean and median of relative errors between averaged estimated velocities and measured velocities. The means, 3.53% for Vp and 2.51% for Vs, and the medians, 2.83% for Vp and 2.12% for Vs, of relative errors indicate that estimated velocities reliably reproduce sonic logs, even if the model is isotropic. As expected, the non-averaged estimated velocities are not suitable for comparison to sonic logs. For example, they do not accurately reproduce measurements at depths xx728 ft and xx815ft whereas spatial averaging of estimated velocities yields to a good agreement with field data. These layers are likely to be thin and stiff, and their properties are spatially averaged during sonic logging.

Figure 4.5 shows the Young's moduli and Poisson's ratios calculated from logs and estimated rock elastic properties. Young's modulus is reproduced accurately: the mean and median of relative errors are 6.1% and 4.6%, respectively. Figure 4.5 also shows the results obtained from the estimation of Poisson's ratio. Although the mean and median of relative errors are not large (8.3% and 5.7%, respectively), the qualitative match with the field-obtained Poisson's ratio is poor (as it is the case from xx750 ft to xx790 ft, for instance). Because of this behavior, Poisson's ratio is not used in the interpretation. Section 4.4 discusses the sensitivity of Young's modulus and Poisson's ratio to measurement errors.

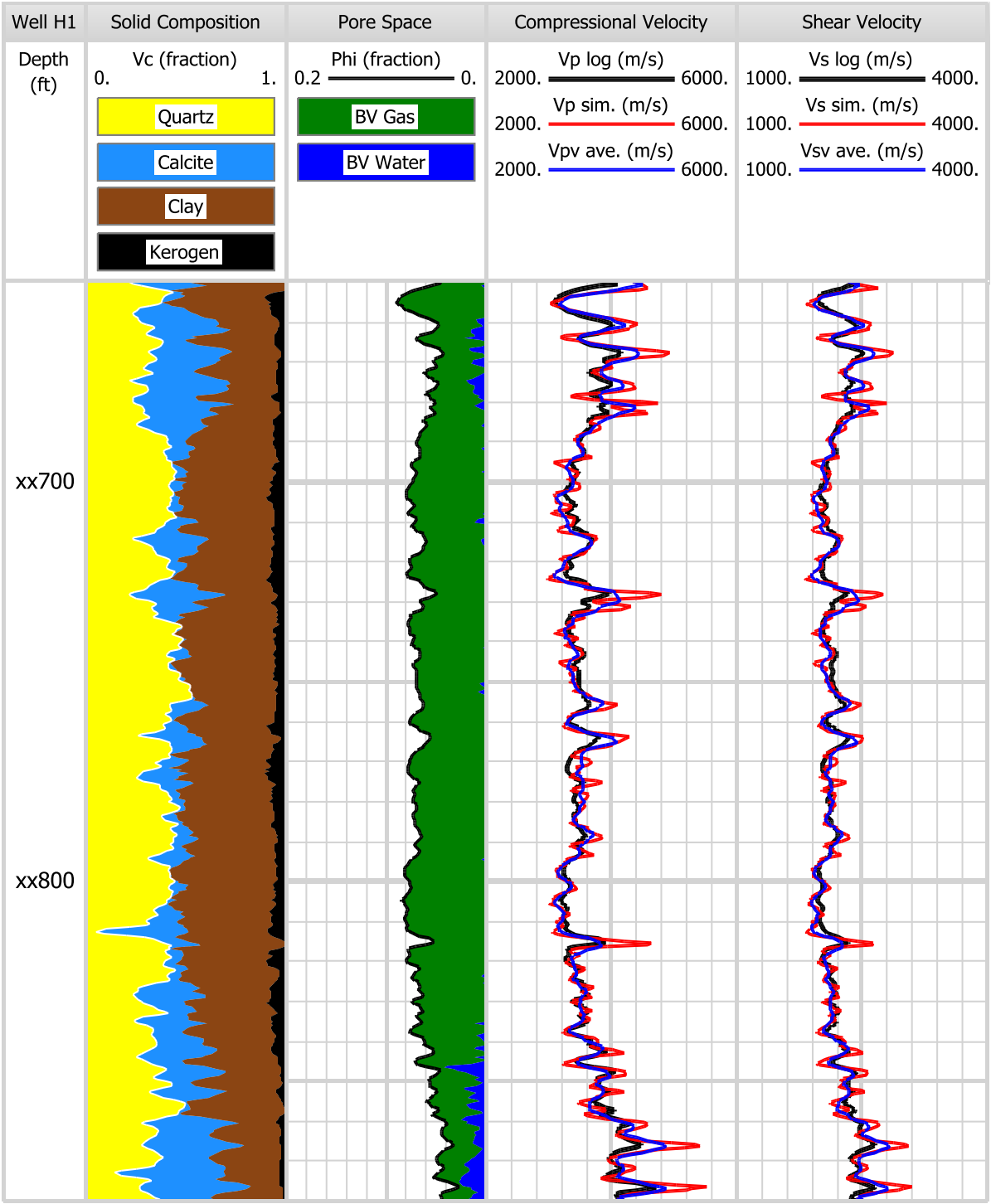
Well H1
Solid Composition
Pore Space
Compressional Velocity
Shear Velocity
Depth (ft)
Vc (fraction)
0.
1.
Quartz
Calcite
Clay
Kerogen
Phi (fraction)
0.2
0.
BV Gas
BV Water
Vp log (m/s)
2000.
6000.
Vp sim. (m/s)
2000.
6000.
Vpv ave. (m/s)
2000.
6000.
Vs log (m/s)
1000.
4000.
Vs sim. (m/s)
1000.
4000.
Vsv ave. (m/s)
1000.
4000.
xx700
xx800

Figure 4.4: Isotropic velocity estimation in Well H1. Track 1: relative depth. Track 2: volumetric composition (Vc) of the solid part of the rock. Track 3: porosity and bulk volume (BV) of water and gas. Track 4: compressional velocity. Track 5: shear velocity. In tracks 4 and 5, black, red, and blue curves identify field, non-averaged estimated, and spatially averaged estimated velocity, respectively. Table 4.1 describes the comparison between estimated and measured velocities.

	Compressional Velocity	**Shear Velocity**
Mean of relative errors	3.53%	2.51%
Median of relative errors	2.83%	2.12%

Table 4.1: Mean and median of relative errors between spatially averaged estimated and measured velocities in Well H1.

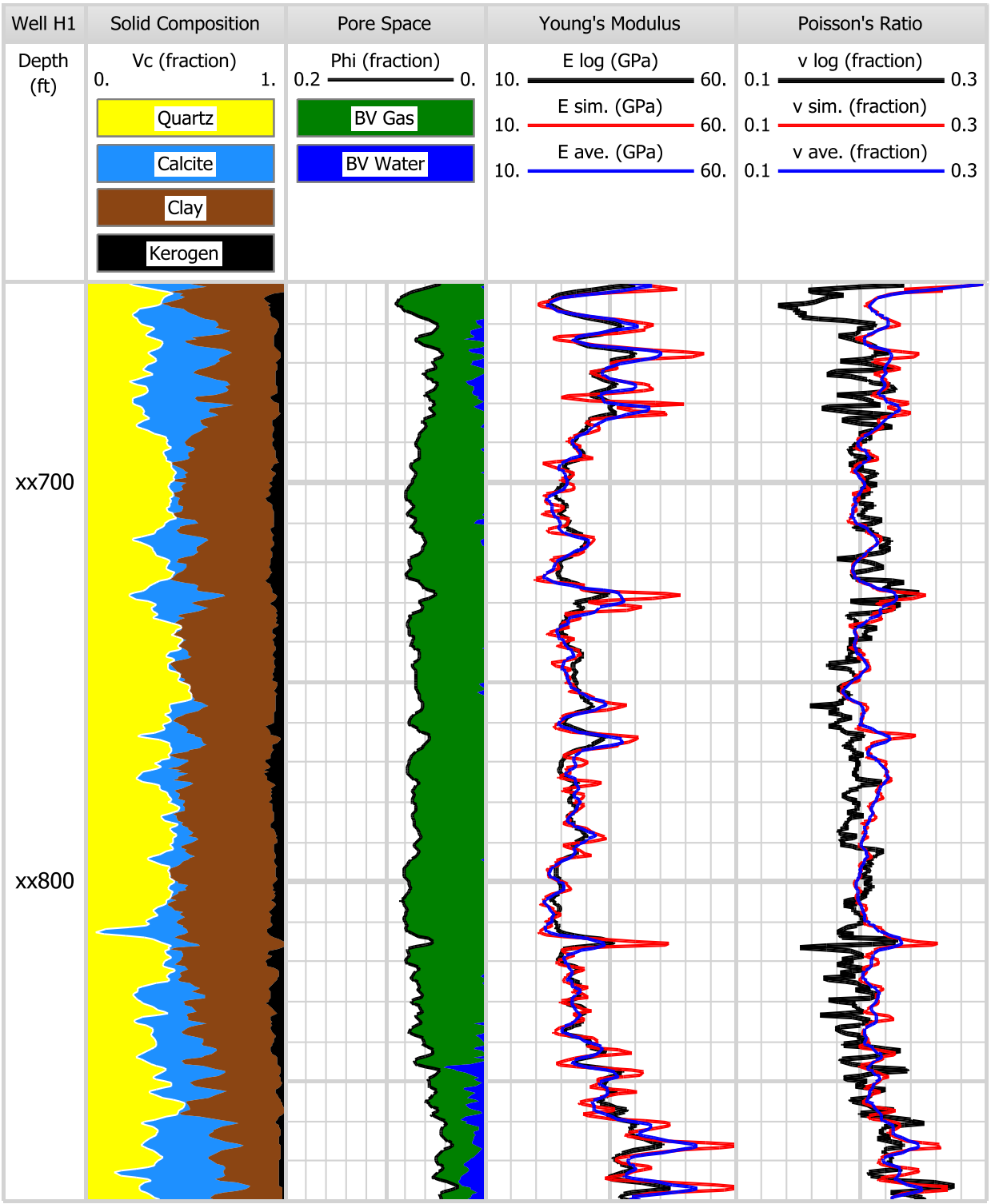
Well H1
Solid Composition
Pore Space
Young's Modulus
Poisson's Ratio
Depth (ft)
Vc (fraction)
0.
1.
Quartz
Calcite
Clay
Kerogen
Phi (fraction)
0.2
0.
BV Gas
BV Water
E log (GPa)
10.
60.
E sim. (GPa)
10.
60.
E ave. (GPa)
10.
60.
v log (fraction)
0.1
0.3
v sim. (fraction)
0.1
0.3
v ave. (fraction)
0.1
0.3
xx700
xx800

Figure 4.5: Young's modulus and Poisson's ratio in Well H1. Track 1: relative depth. Track 2: volumetric composition (Vc) of the solid part of the rock. Track 3: porosity and bulk volume (BV) of water and gas. Track 4: Young's modulus. Track 5: Poisson's ratio. In tracks 4 and 5, black, red, and blue curves identify field-obtained, non-averaged estimated, and spatially averaged estimated elastic properties, respectively.

4.2.3 Interpretation of results

The rock physics model invoked in Well H1 to estimate rock elastic properties and velocities is isotropic. However, it is not inferred that the mechanical properties of the formation are isotropic and should not be assumed that horizontal and vertical velocities are equal. The fact that the rock physics model is isotropic and accurately reproduce sonic logs could indicate that rock fabric is not the main cause for anisotropy of rock mechanical properties. It could be due to other factors, such as stress, for example.

The host material is composed of clay and kerogen. Yet, given the small volumetric concentration of organic matter, clay is assumed to be the main load-bearing rock component. Carbonate material is added to the background matrix before quartz; it suggests that calcite may have more influence on rock elastic properties than quartz. Therefore, calcite should be preferred to quartz in cases where identification of stiff, or compliant, depth intervals is based on the volumetric concentration of these minerals.

The formation exhibits large amounts of gas between xx680 ft and xx830 ft—average of total porosity is equal to 7% and gas saturation is more than 95%—. In order to optimize hydrocarbon production, horizontal wells should be drilled within this depth interval. Rock fabric properties are constant throughout the entire depth interval. Consequently, identification of suitable zones for drilling a horizontal well or to contain

fracture propagation is not based on rock fabric. According to Sone and Zoback (2010), the higher the Young's modulus, the less sensitive the formation becomes to creeping behavior. Creep is the tendency of a solid to deform over time under stress and is unsuitable for efficient hydraulic stimulation. This elastic property also correlates with fracturability (Britt and Schoeffler, 2009) and stiffness (Sone and Zoback, 2010). Therefore, identification of suitable zones to drill a horizontal well or to contain fracture propagation is based on Young's modulus. Four layers exhibit a non-averaged estimated Young's modulus value superior to 35 GPa (this value is used as a baseline to identify stiff rocks in the production interval). They are located at xx720 ft, xx755 ft, xx765 ft, and xx815 ft. The stiff layers at xx755 ft and xx765 ft are the best targets to drill a horizontal well and initiate hydraulic stimulation because they are placed in the middle of the production interval, and would therefore enable gas production from above and below. The stiff rocks at xx720 ft and xx815 ft may act as fracture containments, i.e. they might arrest the propagation of hydraulic fractures.

4.3 WELL H2

This section describes the application of the rock physics simulation and interpretation method in Well H2. The rock physics model constructed in Well H1 is invoked to estimate rock elastic properties and velocities. Simulation results are discussed and used to assess suitable zones for drilling a horizontal well and favorable intervals to initiate or contain hydraulic fractures.

4.3.1 Mineralogy and rock physics model

Figure 4.6 shows the estimations of rock solid composition, porosity, and fluid saturations in Well H2. The interval of study, from xx060 ft to xx290 ft, corresponds to the Haynesville shale, with part of the transition to the Haynesville limestone at the bottom. Additional minerals may be present in small amounts, but only main constituents are used in the simulations. The formation exhibits an overall constant volume of kerogen (mean of kerogen volumetric concentration is 5%), but it contains a few non-organic intervals (at xx100 ft, for example). Volumetric concentration of quartz tends to correlate with clay content, decreasing as volumetric concentration of carbonate increases.

The rock physics model constructed in Well H1 is used to estimate rock elastic properties and velocities. The host comprises clay and kerogen. Next, calcite is added, followed by quartz. All solids are modeled as spheres. Pore aspect ratio is the only parameter that changes in the simulations and is assumed to be equal to 0.06.

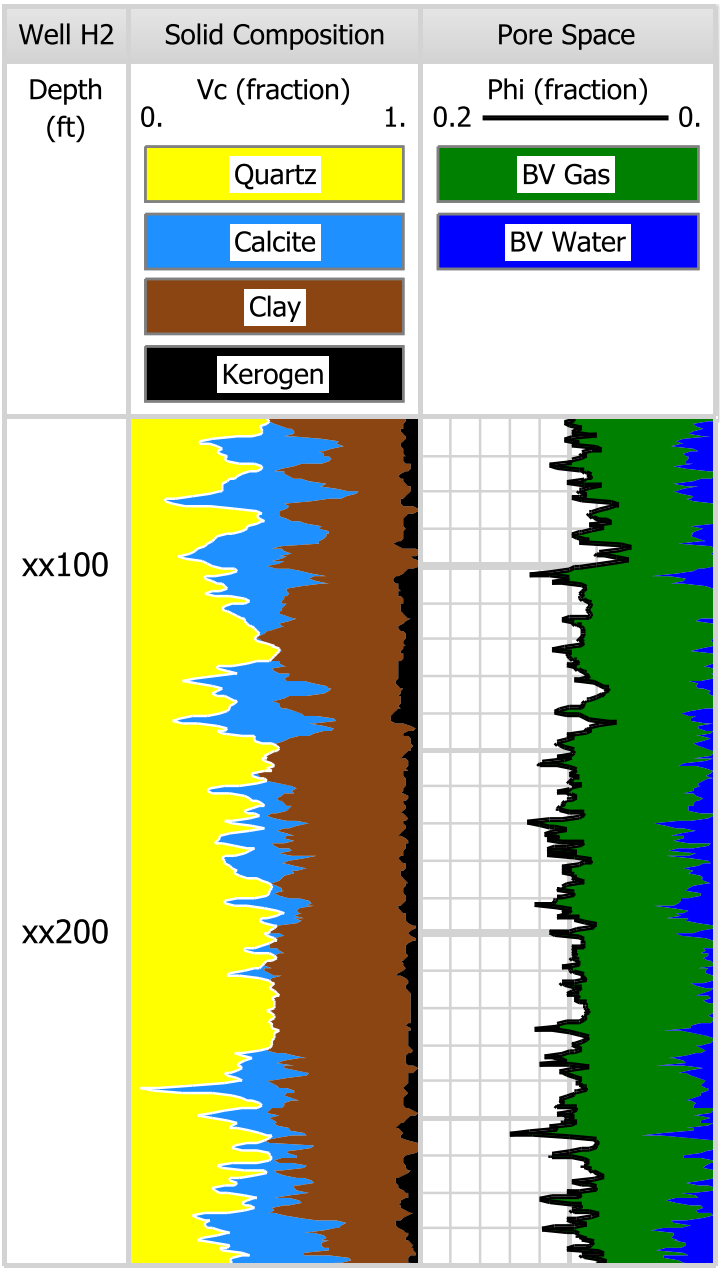

Figure 4.6: Rock composition in Well H2. Track 1: relative depth. Track 2: volumetric composition (Vc) of the solid part of the rock. Track 3: porosity and bulk volume (BV) of water and gas.

4.3.2 Simulation results

Figure 4.7 shows the results obtained from velocity estimation, describing both non-averaged and spatially averaged estimations. Table 4.2 describes the mean and median of relative errors between spatially averaged estimated and measured velocities. The mean, 2.94 % for Vp and 2.07% for Vs, and the median, 3.11% for Vp and 2.25% for Vs, of relative errors show that estimated velocities reliably reproduce sonic logs, except in a few carbonate-rich intervals (at xx070 ft, xx080 ft, and xx090 ft, for instance).

Figure 4.8 shows Young's modulus and Poisson's ratio calculated from logs and from estimated rock elastic properties. Young's modulus is reproduced accurately and mean and median of relative errors are 6.0% and 3.9%, respectively. Figure 4.8 also shows results obtained from the estimation of Poisson's ratio. Although the mean and median of relative errors—6.1% and 4.5%, respectively—are similar to the ones of Young's modulus, the qualitative match with field-obtained Poisson's ratio is poor, especially from xx145 ft to xx160 ft and from xx210 ft to xx230 ft. Therefore, Poisson's ratio is not used in the interpretation.

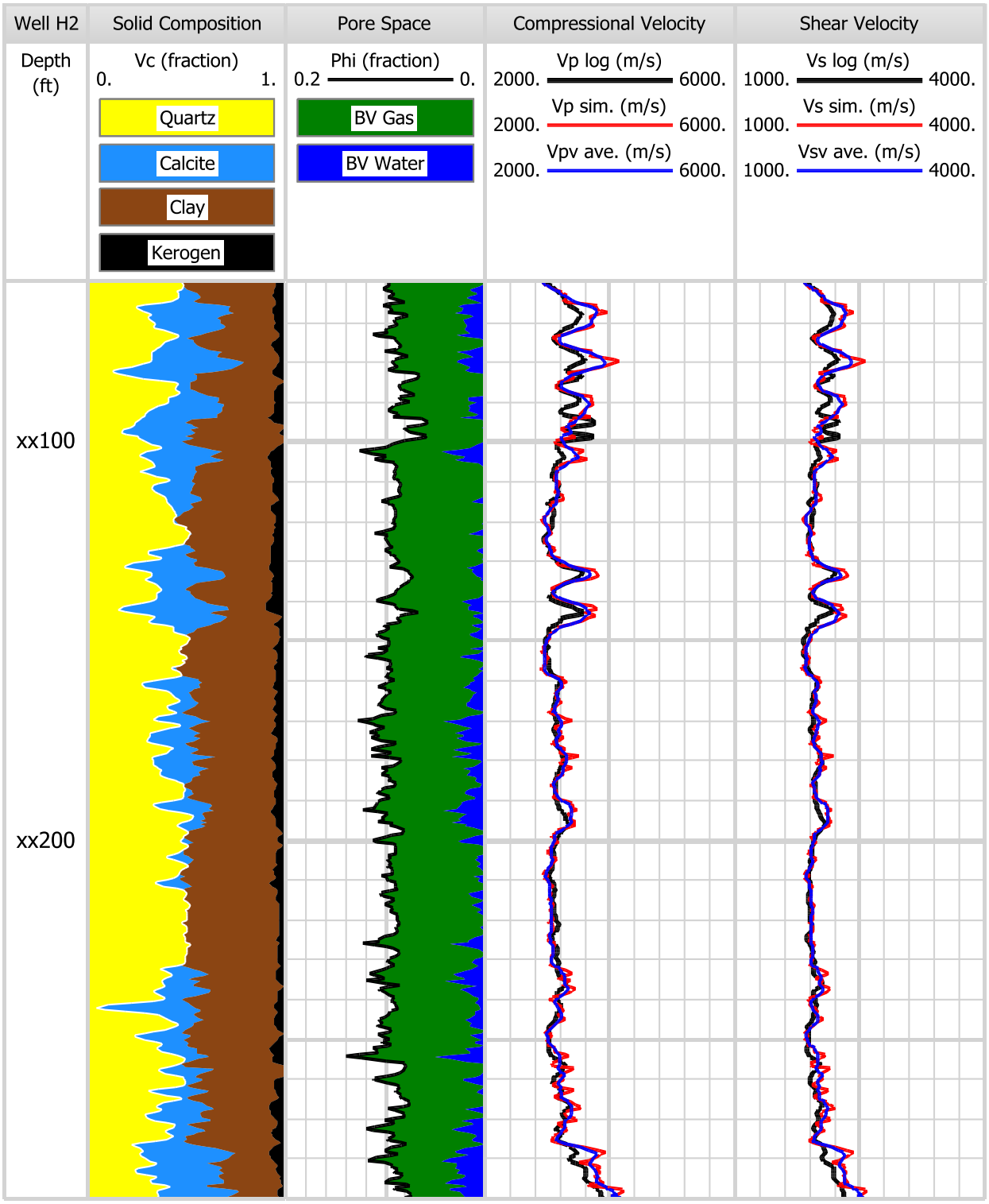
Well H2
Solid Composition
Pore Space
Compressional Velocity
Shear Velocity
Depth (ft)
Vc (fraction)
0.
1.
Quartz
Calcite
Clay
Kerogen
Phi (fraction)
0.2
0.
BV Gas
BV Water
Vp log (m/s)
2000.
6000.
Vp sim. (m/s)
2000.
6000.
Vpv ave. (m/s)
2000.
6000.
Vs log (m/s)
1000.
4000.
Vs sim. (m/s)
1000.
4000.
Vsv ave. (m/s)
1000.
4000.
xx100
xx200

Figure 4.7: Isotropic velocity estimation in Well H2. Track 1: relative depth. Track 2: volumetric composition (Vc) of the solid part of the rock. Track 3: porosity and bulk volume (BV) of water and gas. Track 4: compressional velocity. Track 5: shear velocity. In tracks 4 and 5, black, red, and blue curves identify field, non-averaged estimated, and spatially averaged estimated velocity, respectively. Table 4.2 describes comparison between estimated and measured velocities.

	Compressional Velocity	**Shear Velocity**
Mean of relative errors	2.94%	2.07%
Median of relative errors	3.11%	2.25%

Table 4.2: Mean and median of relative errors between spatially averaged estimated and measured velocities in Well H2.

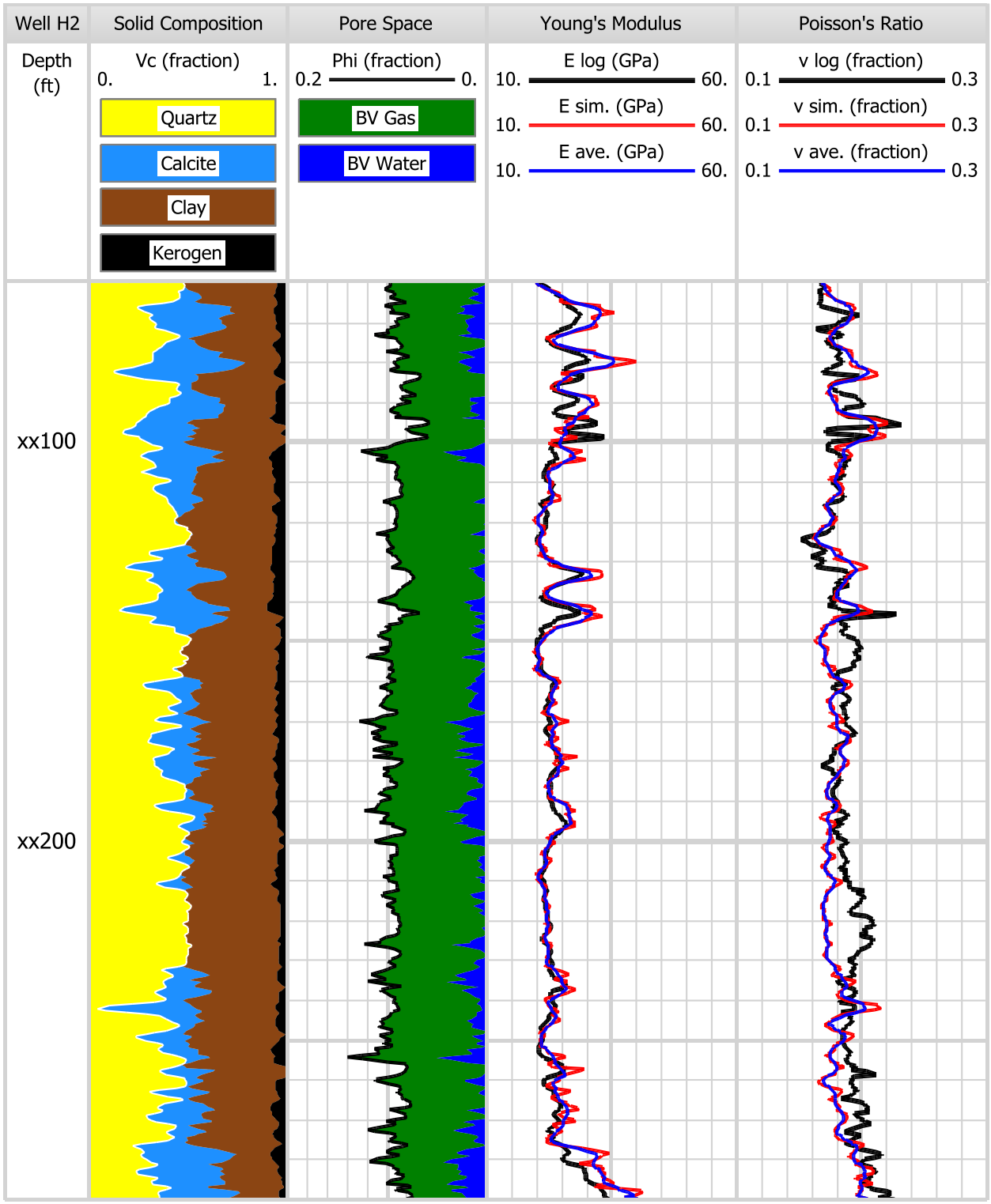
Well H2
Solid Composition
Pore Space
Young's Modulus
Poisson's Ratio
Depth (ft)
Vc (fraction)
0.
1.
Quartz
Calcite
Clay
Kerogen
Phi (fraction)
0.2
0.
BV Gas
BV Water
E log (GPa)
10.
60.
E sim. (GPa)
10.
60.
E ave. (GPa)
10.
60.
v log (fraction)
0.1
0.3
v sim. (fraction)
0.1
0.3
v ave. (fraction)
0.1
0.3
xx100
xx200

Figure 4.8: Young's modulus and Poisson's ratio in Well H2. Track 1: relative depth. Track 2: volumetric composition (Vc) of the solid part of the rock. Track 3: porosity and bulk volume (BV) of water and gas. Track 4: Young's modulus. Track 5: Poisson's ratio. In tracks 4 and 5, black, red, and blue curves identify field-obtained, non-averaged estimated, and spatially averaged estimated elastic properties, respectively.

4.3.3 Interpretation of results

Velocities and Young's modulus are accurately reproduced in Well H2 when the rock physics model constructed in Well H1 is used in the simulations. Rock fabrics are quasi-identical in the two wells, except for pore aspect ratio. Such behavior could suggest lateral homogeneity of the Haynesville shale rock fabric in the area where field data were acquired for analysis. Lateral homogeneity of the Haynesville shase is discussed in section 4.5.

The rock fabric in Well H2 is similar to the one in Well H1. Therefore, analysis of rock fabric properties is identical. The host material is composed of clay and kerogen. Yet, given the low volumetric concentration of organic matter, clay is assumed to be the main load-bearing rock component. Carbonate material is added to the background matrix before quartz. It suggests that calcite may have more influence on rock elastic properties than quartz. Therefore, calcite should be preferred to quartz in cases where identification of stiff or compliant depth intervals is based on the volumetric concentration of these minerals. Rock fabric properties are constant throughout the entire simulation interval.

A Young's modulus value of 30 GPa is chosen to identify stiff zones in Well H2 (rock fabric is vertically homogeneous, and therefore not used in the interpretation). Consequently, two suitable layers for drilling horizontal wells are identified in the middle

of the formation—where hydraulic stimulation will enable gas production from above and below—; the first one is located at xx133 ft and the second one at xx143 ft. The stiff rocks above xx100 ft are likely to arrest the propagation of hydraulic fractures. Similar containment behavior is expected to occur below xx277 ft. It suggests that fractures initiated during hydraulic stimulation are likely to remain within the Haynesville shale depth interval.

4.4 Sensitivity of Young's Modulus and Poisson's Ratio to Measurement Errors

Although Young's moduli were reliably reproduced in Wells H1 and H2, simulated Poisson's ratios did not agree well with those calculated from field data. This section discusses the sensitivity of the two elastic properties to measurement errors in compressional- and shear-wave velocities.

Young's modulus and Poisson's ratio can be expressed as functions of compressional and shear velocities, in addition to bulk density in the case of Young's modulus. Young's modulus is given by

$$E = \frac{3\,\rho\,V_p{}^2\,V_s{}^2 - 4\,\rho\,V_s{}^4}{\left(V_p{}^2 - V_s{}^2\right)} = \frac{9\,K\,\mu}{3\,K + \mu}, \tag{4.1}$$

and Poisson's ratio by

$$\nu = \frac{V_p{}^2 - 2\,V_s{}^2}{2\left(V_p{}^2 - V_s{}^2\right)} = \frac{3\,K - 2\,\mu}{2\,(3\,K + \mu)}. \tag{4.2}$$

Assuming isotropic elastic properties, the ratio of relative variation of Young's modulus over relative variation of compressional velocity is given by

$$\frac{\Delta E/E}{\Delta V_p/V_p} = \frac{2\,V_p^{\,2}\,V_s^{\,2}}{\left(V_p^{\,2} - V_s^{\,2}\right)\left(3\,V_p^{\,2} - 4\,V_s^{\,2}\right)}. \tag{4.3}$$

Similarly the ratio of relative variation of Young's modulus over relative variation of shear velocity is given by

$$\frac{\Delta E/E}{\Delta V_s/V_s} = \frac{6\,V_p^{\,4} - 16\,V_p^{\,2}\,V_s^{\,2} + 8\,V_s^{\,4}}{\left(V_p^{\,2} - V_s^{\,2}\right)\left(3\,V_p^{\,2} - 4\,V_s^{\,2}\right)}. \tag{4.4}$$

In the case of Poisson's ratio, the ratio of relative variation over relative variation of compressional velocity is given by

$$\frac{\Delta \nu/\nu}{\Delta V_p/V_p} = \frac{2\,V_p^{\,2}\,V_s^{\,2}}{\left(V_p^{\,2} - V_s^{\,2}\right)\left(V_p^{\,2} - 2\,V_s^{\,2}\right)}. \tag{4.5}$$

Finally, the ratio of relative variation of Poisson's ratio over relative variation of shear velocity is given by

$$\frac{\Delta \nu/\nu}{\Delta V_s/V_s} = \frac{-2\,V_p^{\,2}\,V_s^{\,2}}{\left(V_p^{\,2} - V_s^{\,2}\right)\left(V_p^{\,2} - 2\,V_s^{\,2}\right)}. \tag{4.6}$$

Variations of Young's modulus and Poisson's ratio due to variation of field compressional- and shear-wave velocities are calculated in Wells H1 and H2, along the depth intervals of interest. Table 4.3 summarizes the median of Young's modulus and Poisson's ratio variations due to variations of compressional and shear velocities.

	Well H1	Well H2
$\frac{\Delta E/E}{\Delta V_p/V_p}$	0.80	0.86
$\frac{\Delta E/E}{\Delta V_s/V_s}$	1.2	1.1
$\frac{\Delta \nu/\nu}{\Delta V_p/V_p}$	4.8	5.5
$\frac{\Delta \nu/\nu}{\Delta V_s/V_s}$	-4.8	-5.5

Table 4.3: Median of Young's modulus and Poisson's ratio variations due to variations of compressional and shear velocities in Wells H1 and H2. Calculated values are dimensionless.

In Well H1, Poisson's ratio is approximately 6 times more sensitive to errors from compressional velocity than Young's modulus, and approximately 4 times (in absolute value) more sensitive to errors from shear velocity than Young's modulus. In Well H2, Poisson's ratio is approximately 6.4 times more sensitive to errors from compressional velocity than Young's modulus, and approximately 4.8 times (in absolute value) more sensitive to errors from shear velocity than Young's modulus.

Poisson's ratio estimation in the Haynesville shale yields poor agreement with field data. Poor qualitative matches between estimated and field-obtained Poisson's ratios suggest that interpretation should not be based on estimated values of this elastic property. Additionally, Young's moduli calculated from logs are accurately reproduced in the simulations. Therefore, Young's modulus is preferred to Poisson's ratio in the interpretation, in both Well H1 and H2. This choice is supported by the results of the sensitivity analysis developed in this section because they confirm the higher sensitivity of Poisson's ratio to errors in sonic measurements compared to Young's modulus.

Results of sensitivity analysis of Young's modulus and Poisson's ratio to measurement errors also question the use of these rock elastic properties derived from field data. Acoustic waveforms acquired by sonic tools are processed to obtain sonic logs. Such signal-processing operation is complex, and errors in compressional- and shear-wave velocity logs can be expected in the process. Due to its low sensitivity to errors in velocities, Young's modulus calculated from field measurements is assumed to be accurate. On the contrary, high Poisson's ratio sensitivity to errors in velocities suggests that, when computed from field data, this elastic property should be interpreted with caution. Poisson's ratio calculated from logs should be validated with core measurements before interpretation. Nevertheless, cores brought to surface experience temperature and pressure variations, and may exhibit rock elastic properties that differ from in-situ properties.

4.5 SUMMARY

Velocities and Young's modulus are accurately reproduced in Well H2 when the rock physics model constructed in Well H1 is used in the simulations. Rock fabrics are

shown to be quasi-identical in the two wells, except for pore aspect ratio—it exhibits a value of 0.07 in Well H1 and 0.06 in Well H2—. Such variation of pore aspect ratio could indicate a larger compaction stress in Well H2 compared to the one in Well H1 (pores are expected to flatten as stress increases). This hypothesis is supported by the fact that Haynesville shale is located in a deeper depth interval in Well H2 than in Well H1 (compaction stress usually increases with depth). All remaining rock fabric properties are identical in the two wells. Such a behavior suggests that the rock fabric of the Haynesville shale is likely to be laterally homogeneous in the area—where field data were acquired for analysis.

Even though the rock physics model invoked in the two wells is isotropic, the Haynesville shale is not assumed to exhibit isotropic compressional- and shear-wave velocities. However, it suggests that rock fabric is not the main cause of anisotropy. Anisotropy, if present, could be due to other factors, such as stress, for example.

Identification of favorable production intervals is based on porosity and gas saturation. Rock fabrics are vertically homogeneous, and therefore not used to assess suitable zones to drill horizontal wells or contain hydraulic fractures. Determination of such zones is based on Young's modulus. For optimum gas yielding, recommended emplacements for drilling horizontal wells are located in the middle of a production interval. Stiff layers from which hydraulic fractures are not initiated are potential fracture containments.

Chapter 5: Barnett Shale Case Study

This chapter describes the application of the previously described simulation and interpretation method in the Barnett shale formation. The Barnett shale is one of the first hydrocarbon-bearing shale where horizontal drilling and hydraulic stimulation enabled economically viable production of hydrocarbons. The purpose of this chapter is to quantify rock fabric properties in two wells and use the results to identify suitable zones for drilling horizontal wells and depth intervals to initiate or contain hydraulic fractures.

5.1 Background of the Barnett Shale

The Barnett shale, located in north Texas, became one of the first gas play in the United States after the successful development of horizontal drilling and hydraulic fracturing. Estimation of elastic properties and velocities is more difficult in the Barnett shale than in the Haynesville shale: rock fabric is more spatially variable, and several rock constituents exhibit an anisotropic distribution. Therefore, rock typing and anisotropic rock physics models must be invoked in the simulations. Because Young's modulus and Poisson's ratio assume isotropic elastic properties, they are not suitable in the interpretation.

Barnett shale was deposited during the Mississippian. In the northern and northeastern regions it overlies the Viola/Simpson group, a stiff limestone formation that acts as fracture barrier. On the other hand, in the southern and southwestern regions the Barnett shale overlies Chappel limestone or Ellenburger dolomite/limestone (Montgomery et al., 2005). This last formation is porous and water-saturated, and is avoided during hydraulic stimulation to prevent water production and aquifer contamination. In the south/southwestern regions the Barnett shale consists of a single

depth interval, whereas in north/northeastern regions it is divided into two depth intervals (Montgomery et al., 2005) referred as the upper and lower sections. In between the two sections lies the Forestburg formation, a limestone group that acts as fracture barrier.

5.2 WELL B1

Well B1 is located in the south/southwestern region of the Barnett shale, where it consists of a single depth interval. Due to vertical heterogeneity of rock fabric, rock typing is performed and specific fabric properties are quantified for each rock type. Based on rock composition and fabric, compressional- and shear-wave velocities are simulated with an anisotropic rock physics model. Rock fabric properties are validated when estimated velocities accurately reproduce sonic logs. Results are discussed and used to assess suitable zones for drilling a horizontal well and to initiate or contain hydraulic fractures.

5.2.1 Well logs and mineralogy

Figure 5.1 shows the main well logs acquired in the interval of interest. Low apparent resistivity minima are attributed to pyritic laminae and cause errors in the estimation of rock composition. Some of these laminae are also visible on electric images as thin dark streaks— in this example, electric images get darker as apparent resistivity decreases—. Such intervals are ignored in the interpretation due to unreliable estimated rock composition.

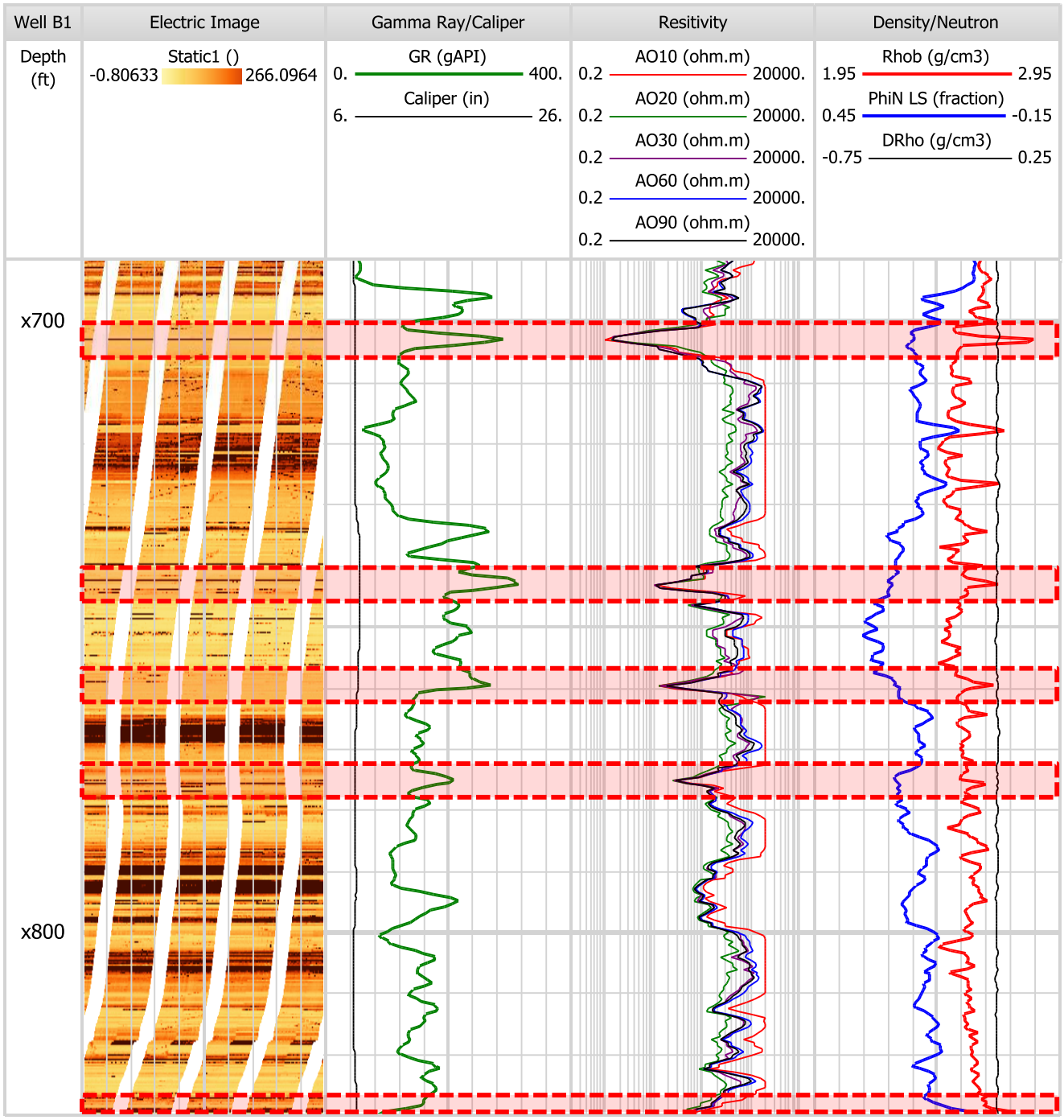
Well B1
Electric Image
Gamma Ray/Caliper
Resitivity
Density/Neutron
Depth (ft)
Static1 ()
-0.80633
266.0964
GR (gAPI)
0.
400.
Caliper (in)
6.
26.
AO10 (ohm.m)
0.2
20000.
AO20 (ohm.m)
0.2
20000.
AO30 (ohm.m)
0.2
20000.
AO60 (ohm.m)
0.2
20000.
AO90 (ohm.m)
0.2
20000.
Rhob (g/cm3)
1.95
2.95
PhiN LS (fraction)
0.45
-0.15
DRho (g/cm3)
-0.75
0.25
x700
x800

Figure 5.1: Main logs in Well B1. Track 1: relative depth. Track 2: electric images. Track 3: gamma-ray and caliper logs. Track 4: apparent resistivity logs. Track 5: bulk density, neutron porosity (in limestone units), and delta density logs. Red rectangles indicate depth intervals where rock composition inversion results are unreliable because of abnormal resistivity vales due to pyritic laminae.

Figure 5.2 shows the estimated rock composition. Even though additional minerals may be present in minor amounts—pyrite and ankerite, for example—, only main solid components are displayed and subsequently used in this section. Kerogen volumetric concentration is spatially variable and exhibits high values, as much as 31.8% of rock solid volume at x751 ft. Quartz volumetric concentration is large (mean is equal to 47%) and generally tends to anti-correlate with calcite. Clay volumetric concentration (mean is equal to 28%) is lower than in the Haynesville field cases (volumetric concentration of clay in Well H1 and H2 are equal to 40% and 39%, respectively). Porosity is low, with a median approximately equal to 7%, and abnormally high porosity peaks are due to inversion errors in the presence of pyritic laminae (Adiguna, 2012), as shown at the depths x703 ft, x742 ft, x759 ft, x776 ft, and x829 ft. Calcite and dolomite were grouped into a unique component to reduce uncertainty in inversion results, but because both exhibit different elastic properties, slightly different results could be obtained if instead they were inverted separately. Considering the volume of dolomite indicated by XRD data, the impact of such grouping on elastic properties estimations is assumed to be negligible and, therefore, to have no measurable impact on interpretation of results.

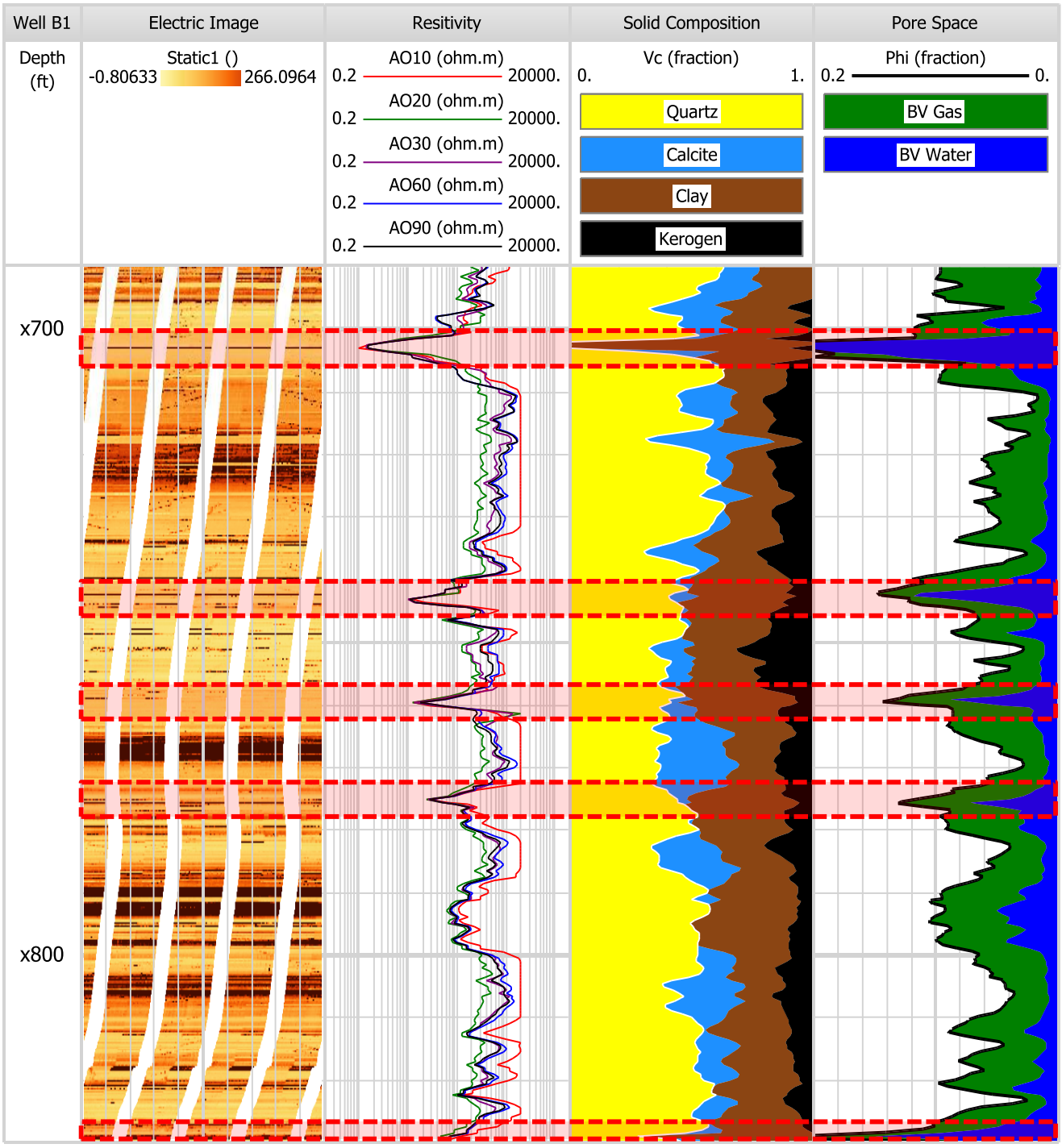
Well B1
Electric Image
Resitivity
Solid Composition
Pore Space
Depth (ft)
Static1 ()
-0.80633
266.0964
AO10 (ohm.m)
AO20 (ohm.m)
AO30 (ohm.m)
AO60 (ohm.m)
AO90 (ohm.m)
0.2
20000.
Vc (fraction)
0.
1.
Quartz
Calcite
Clay
Kerogen
Phi (fraction)
0.2
0.
BV Gas
BV Water
x700
x800

Figure 5.2: Rock composition in Well B1. Track 1: relative depth. Track 2: electric image. Track 3: apparent resistivity logs. Track 4: volumetric composition (Vc) of the solid part of the rock. Track 5: porosity and bulk volume (BV) of water and gas. Red rectangles indicate depth intervals where inversion results are unreliable because of abnormal resistivity values due to pyritic laminae.

5.2.2 Rock typing

Similarly to the Haynesville shale, a vertically uniform isotropic model for the Barnett was invoked first. Inaccurate velocity estimations suggested that the Barnett shale rock fabric is more complex than in Haynesville, and rock typing is required to accurately estimate elastic properties and velocities. Rock fabric is assumed to vary with rock composition. Cluster analysis of volumetric concentration of quartz, calcite, and kerogen in the solid phase of the rock is invoked to perform rock typing. This method is applied with the software Interactive Petrophysics™. Five rock types are identified in Well B1. Table 5.1 describes the average volumetric concentrations of quartz, kerogen, and calcite in the solid part of the rock. Figure 5.3 shows the corresponding rock types in the interval of interest. Locations where porosity is higher than 12% are not taken into account in the interpretation because they correspond to abnormally low resistivity values, where inversion results are unreliable.

	Quartz	Kerogen	Calcite
Rock Type 1	37%	11%	30%
Rock Type 2	41%	20%	15%
Rock Type 3	50%	7%	15%
Rock Type 4	55%	12%	3%
Rock Type 5	64%	0%	13%

Table 5.1: Average volumetric concentration of quartz, kerogen, and calcite in the solid part of the rock for each rock type in Well B1.

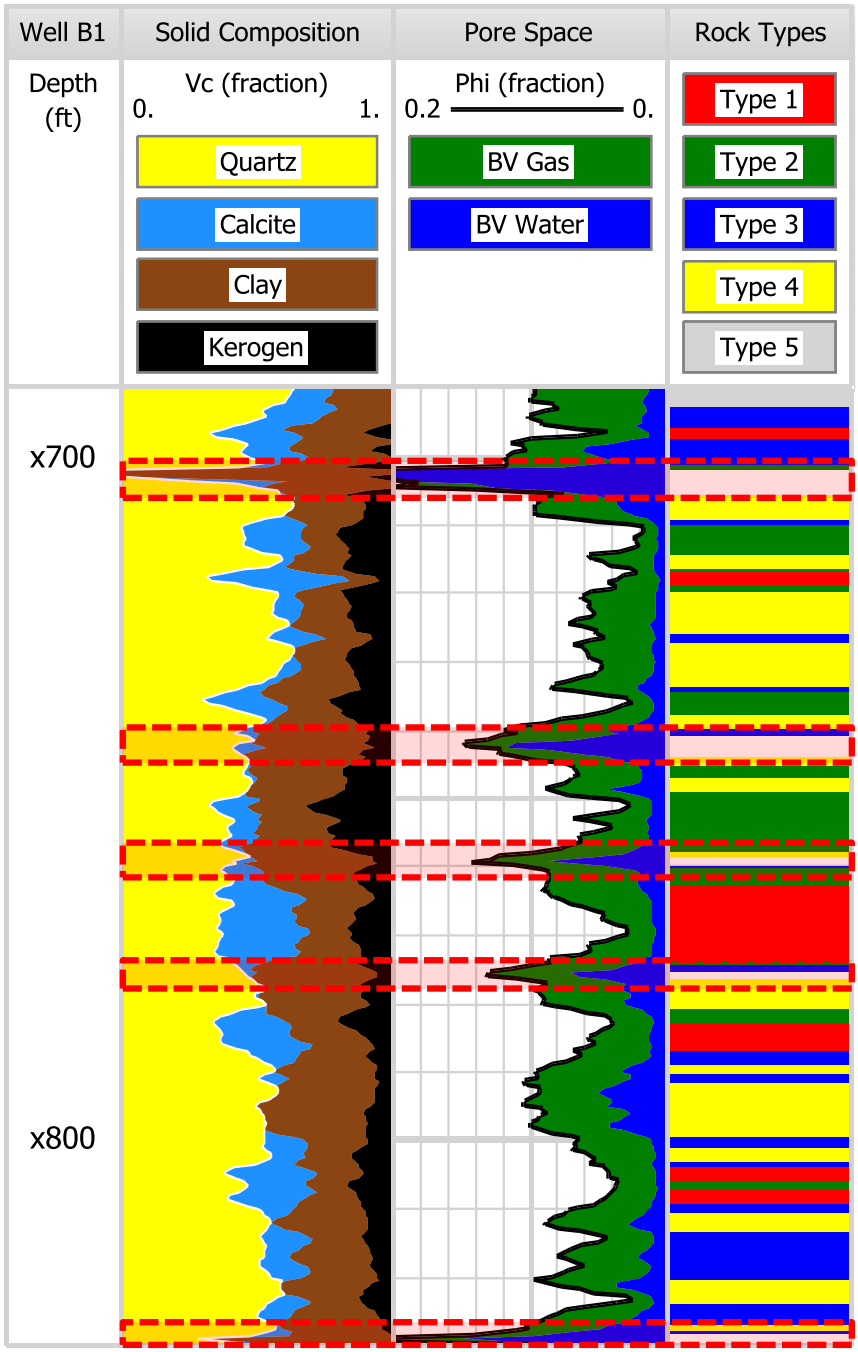

Figure 5.3: Rock typing based on mineral composition in Well B1. Track 1: relative depth. Track 2: volumetric composition (Vc) of the solid part of the rock. Track 3: porosity and bulk volume (BV) of water and gas. Track 4: rock types.

Rock type 1 arises in depth intervals with large calcite volumetric concentration, relatively low quartz volumetric concentration (compared to the remaining of the formation), and medium kerogen volumetric concentration. Calcareous shells are abundant. Rock type 2 exhibits large volumetric concentration of kerogen. Volume of quartz is relatively low and calcite volumetric concentration is average. Rock type 3 exhibits a larger volumetric concentration of quartz than previous rock types, but low volumes of organic matter. Calcite volumetric concentration is similar to the one in rock type 2. This rock type is commonly present in the lower parts of the well, which takes place in the transition to an organic-poor formation. Rock type 4 exhibits large volumetric concentration of quartz and average volumes of organic matter. Calcite volumetric concentration is low. Rock type 5 is only present at the top of Well B1, and corresponds to the end of the transition from an organic-poor formation. It is a non-organic, silica-rich interval.

5.2.3 Isotropic rock physics model

A specific workflow is invoked to construct the isotropic solid rock frame for each rock type. Table 5.2 describes the host materials and the order in which inclusions are added to the background matrix. All components are assumed to exhibit a spherical shape.

	Rock Type 1	Rock Type 2	Rock Type 3	Rock Type 4	Rock Type 5
Host	Clay and Kerogen	Kerogen	Clay	Clay and Kerogen	Clay and Quartz
1st inclusion	Calcite	Clay	Quartz	Quartz	Calcite
2nd inclusion	Quartz	Quartz	Calcite	Calcite	/
3rd inclusion	/	Calcite	Kerogen	/	/
4th inclusion	Porosity	Porosity	Porosity	Porosity	Porosity

Table 5.2: Host and inclusion order for each rock type. The SCA and DEM combination method is invoked when the host is composed of two components. All inclusions are added using the DEM. Porosity is added in the last step. All inclusions exhibit a spherical shape.

5.2.4 Isotropic simulation results

Figure 5.4 shows the results obtained from velocity estimation, describing both non-averaged and spatially averaged estimations. Table 5.3 describes the mean and median of relative errors between spatially averaged estimated and measured velocities. Shear velocity is accurately reproduced—the median of relative errors is 2.55%—whereas compressional velocity estimation is not as reliable—the median of relative errors is 4.90%—. Compressional-wave velocity is especially overestimated in three depth intervals: between x705 ft and x740 ft, between x745 ft and x757 ft, and between

x800 ft and x825 ft. In these depth intervals, the shear velocity log is accurately reproduced with the isotropic rock physics model and estimated compressional velocity values are too high compared to field measurements. This behavior suggests presence of horizontal rock components and/or pores. Section 5.2.5 is intended to model horizontal carbonate shells and horizontal thin compliant pores in order to improve the agreement with field measurements.

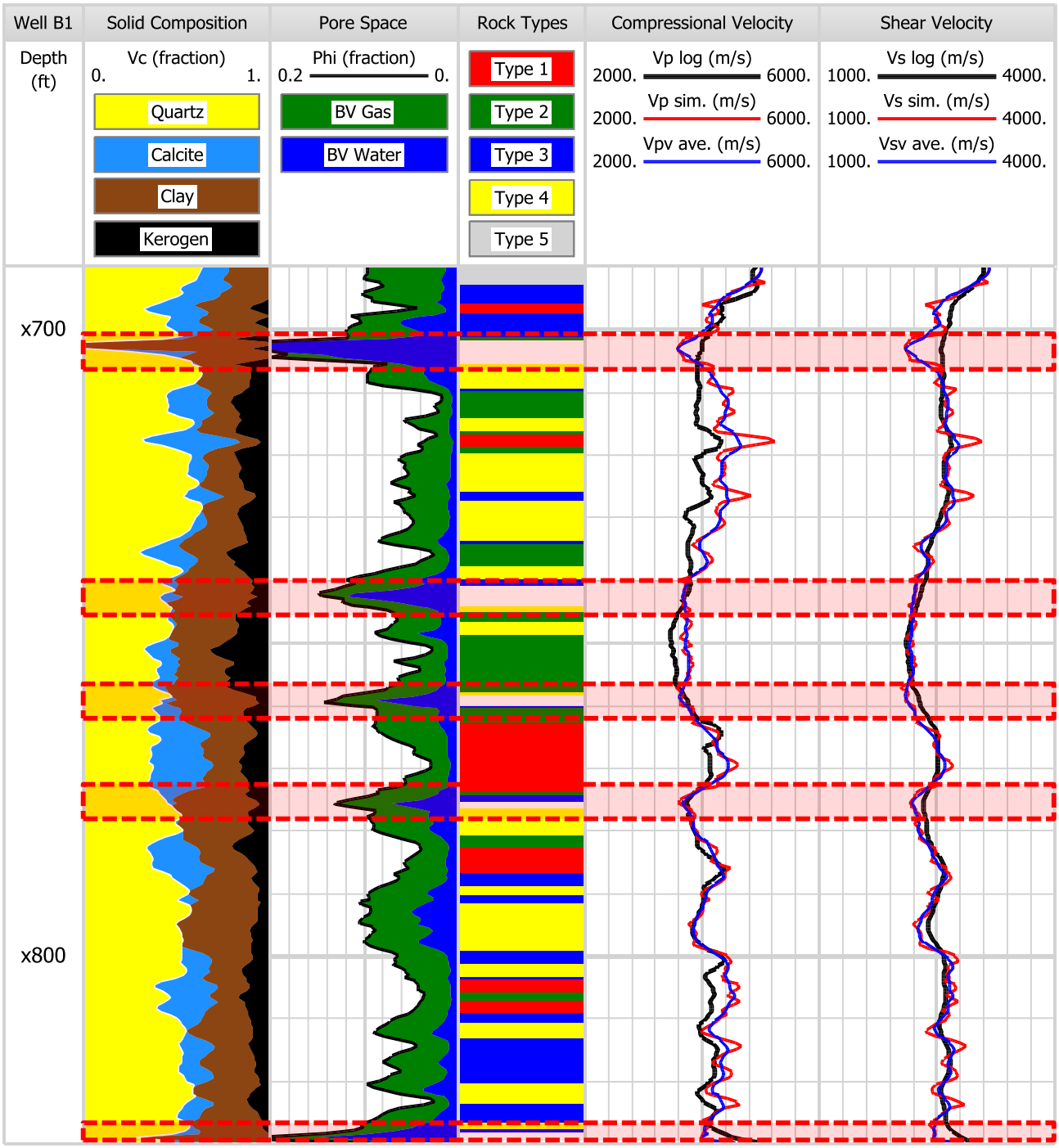
Well B1
Solid Composition
Pore Space
Rock Types
Compressional Velocity
Shear Velocity
Depth (ft)
Vc (fraction)
0.
1.
Quartz
Calcite
Clay
Kerogen
Phi (fraction)
0.2
0.
BV Gas
BV Water
Type 1
Type 2
Type 3
Type 4
Type 5
Vp log (m/s)
2000.
6000.
Vp sim. (m/s)
2000.
6000.
Vpv ave. (m/s)
2000.
6000.
Vs log (m/s)
1000.
4000.
Vs sim. (m/s)
1000.
4000.
Vsv ave. (m/s)
1000.
4000.
x700
x800

Figure 5.4: Isotropic velocity estimation in Well B1. Track 1: relative depth. Track 2: volumetric composition (Vc) of the solid part of the rock. Track 3: porosity and bulk volume (BV) of water and gas. Track 4: rock types. Track 5: compressional velocity. Track 6: shear velocity. In tracks 5 and 6, black, red, and blue curves identify field, non-averaged estimated, and spatially averaged estimated velocity, respectively. Table 5.3 describes comparison between simulated and measured velocities.

	Compressional Velocity	**Shear Velocity**
Mean of relative errors	5.22%	3.20%
Median of relative errors	4.90%	2.55%

Table 5.3: Mean and median of relative errors between spatially averaged isotropic estimated and measured velocities in Well B1.

5.2.5 Anisotropic rock physics model

Identical rock types to those of the isotropic case are used in the anisotropic simulations, except that associated rock fabrics are refined to account for presence of horizontal calcareous shells and compliant pores. The isotropic part of the rock is modeled using the same hosts and inclusion orders than in the isotropic case, but fractions of calcite and porosity are not included in the simulation. These fractions are subsequently added to the isotropic matrix as horizontal inclusions or cracks with Hudson's model. The anisotropic Gassmann fluid-substitution formulation is invoked to estimate saturated rock elastic properties and velocities. Table 5.4 describes fractions of calcite and porosity modeled as horizontal inclusions or cracks and their corresponding

aspect ratio. Different values of crack aspect ratio above and below x770 ft are invoked for rock types 3 and 4.

	Percentage of calcite modeled as horizontal inclusions	Percentage of porosity modeled as horizontal cracks	Calcite inclusions aspect ratio	Porous cracks aspect ratio
Rock Type 1	10%	5%	0.1	0.3
Rock Type 2	5%	5%	0.1	0.1
Rock Type 3 above x770 ft	5%	5%	0.1	0.2
Rock Type 3 below x770 ft				0.3
Rock Type 4 above x770 ft	5%	5%	0.1	0.1
Rock Type 4 below x770 ft				0.3
Rock Type 5	0%	0%	N/A	N/A

Table 5.4: Cracks and inclusions associated with each rock type in Well B1. All inclusions and cracks are horizontal.

5.2.6 Anisotropic simulation results

Figure 5.5 describes the results obtained from velocity estimation, showing both non-averaged and spatially averaged estimations. Estimated velocities, both non-averaged and spatially averaged, describe velocities of propagation in the vertical direction. Table 5.5 describes the mean and median of relative errors between averaged estimated velocities and measured velocities. The estimated shear velocity yields a similar agreement with measurements to the one obtained with isotropic simulation. Estimated compressional velocity is especially improved in depth intervals where it was overestimated with the isotropic rock physics model.

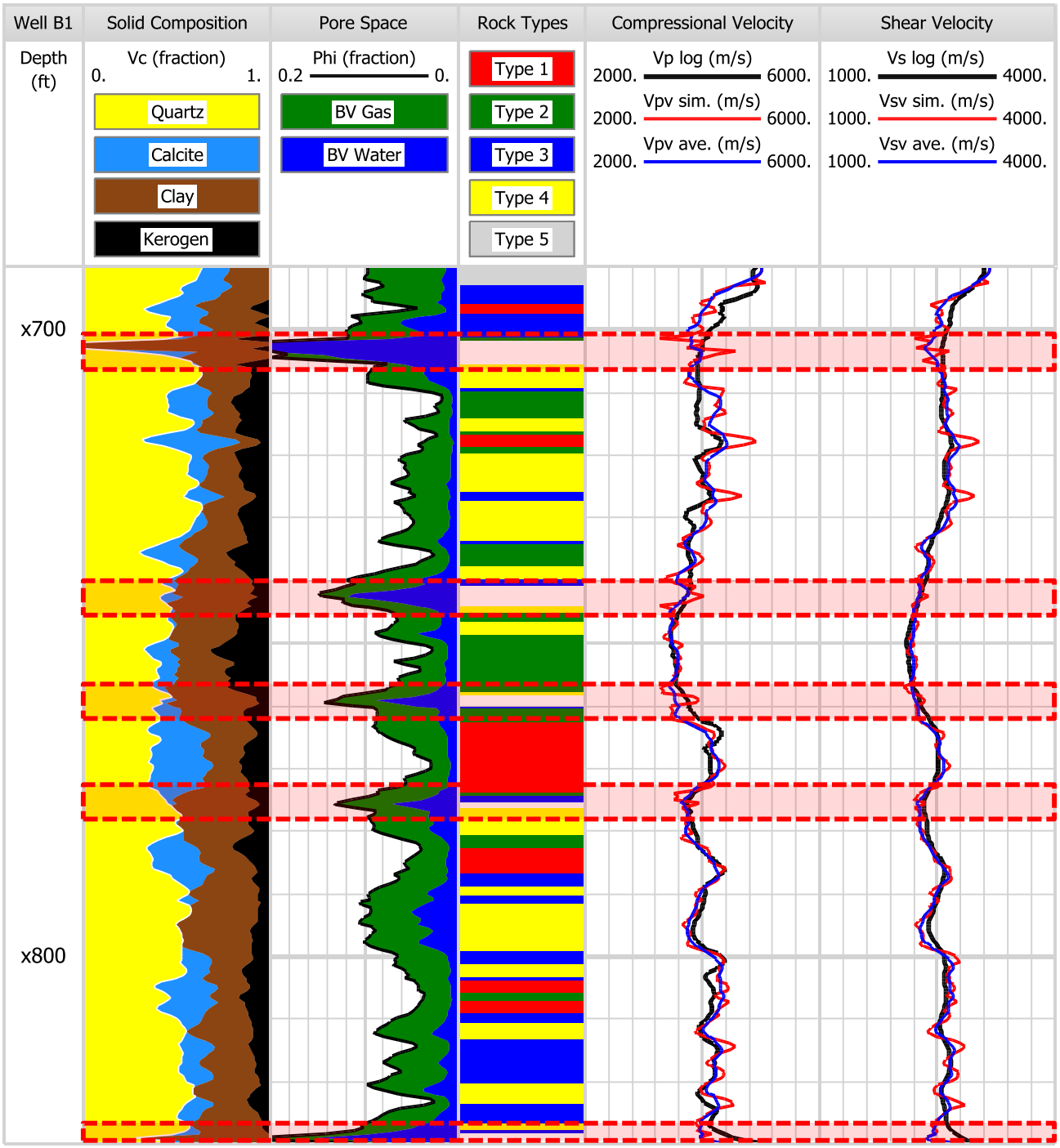
Well B1
Solid Composition
Pore Space
Rock Types
Compressional Velocity
Shear Velocity
Depth (ft)
Vc (fraction)
0.
1.
Quartz
Calcite
Clay
Kerogen
Phi (fraction)
0.2
0.
BV Gas
BV Water
Type 1
Type 2
Type 3
Type 4
Type 5
Vp log (m/s)
2000.
6000.
Vpv sim. (m/s)
2000.
6000.
Vpv ave. (m/s)
2000.
6000.
Vs log (m/s)
1000.
4000.
Vsv sim. (m/s)
1000.
4000.
Vsv ave. (m/s)
1000.
4000.
x700
x800

Figure 5.5: Anisotropic velocity estimation in Well B1. Track 1: relative depth. Track 2: volumetric composition (Vc) of the solid part of the rock. Track 3: porosity and bulk volume (BV) of water and gas. Track 4: rock types. Track 5: compressional velocity. Track 6: shear velocity. In tracks 5 and 6, black, red, and blue curves identify field, non-averaged estimated, and spatially averaged estimated velocity, respectively. Table 5.5 describes comparison between simulated and field velocities.

	Compressional Velocity	**Shear Velocity**
Mean of relative errors	3.50%	2.69%
Median of relative errors	2.55%	2.40%

Table 5.5: Mean and median of relative errors between spatially averaged anisotropic estimated and measured velocities in Well B1.

5.2.7 Interpretation of results

Presence of horizontal cracks is assumed to result from the spatial arrangement of carbonate shells and presence of relatively large volumetric concentrations of organic matter. Kerogen is soft (low bulk and shear moduli compared to other solids), and contributes to deformation of pores because of its low mechanical strength. Factors such as vertical overburden stress are likely to induce horizontal deformation of pores.

With the highest kerogen volumetric concentration, Rock type 2 is the most interesting rock type in terms of hydrocarbon reserves. However, relatively high kerogen content and presence of compliant horizontal cracks indicate that the porous space is subject to deformation, probably due to overburden stress. Therefore, because they present low resistance to collapse, these intervals must be avoided for horizontal well placement. Hydraulic fractures in these intervals could also be subject to embedment, which would decrease their flow conductivity.

Rock types 1 and 4 exhibit average organic content—11% and 12% on average, respectively—and are therefore suitable for production. They differ in their amounts of quartz and calcite. Rock type 4 is silica-rich, whereas Rock type 1 is carbonate-rich. These rock types are more suitable than Rock type 2 to drill horizontal wells because of their stiffer solid frames. Rock type 3 is also suitable for that purpose, but is mainly present at the top and bottom of the depth interval of interest. Therefore, it does not provide a good exposure to hydrocarbon-rich depth intervals. Rock type 1 is more suitable to drill horizontal wells than Rock type 4 because of its low porosity. Low porosity gives rise to a stiffer rock frame, which is less likely to collapse during drilling. The interval with Rock type 1 at x770 ft is a suitable target for drilling a horizontal well as it provides a stiff rock environment and is located between porous hydrocarbon-rich zones. Hydraulic stimulation from this location will enable production from favorable

production depth intervals— with Rock type 1, 2 and 3—above and below. It is also one of the depth intervals with the lowest porosity, highest calcite volumetric concentration, and highest velocities in the middle of the formation. We infer that it could act as a confining interval if hydraulic fractures were initiated from another location. Therefore, this depth interval is considered to be the most suitable one for drilling a horizontal well and to initiate hydraulic stimulation in Well B1.

5.3 WELL B2

Well B2 is located in the north/northeastern region of the Barnett shale. It is here divided into upper and lower depth intervals. The two intervals are separated by a limestone formation that acts as fracture barrier. Electric images indicate presence of natural vertical fractures. Rock typing and anisotropic rock physics model are invoked in the simulations.

5.3.1 Mineralogy and rock typing

Figure 5.6 shows the rock composition and rock typing in the upper depth section of Well B2. Calcite volumetric concentration is large, especially in thick, organic-poor, and clay-poor carbonate intervals (Rock type 3) that exhibit very low porosity (less than 2%), and are almost completely water-saturated (water saturation is more than 95%). Silica-rich intervals contain more clay and kerogen—up to 27% and 17%, respectively—. Water saturation is also high (more than 50%) and the presence of organic content is associated with gas. Three rock types were identified based on volumetric concentrations of quartz, calcite, and kerogen. Table 5.6 describes the average volumetric concentrations of these components in the solid phase of the rock per rock type.

	Quartz	**Kerogen**	**Calcite**
Rock Type 1	50%	8%	21%
Rock Type 2	36%	6%	40%
Rock Type 3	13%	0.5%	81%

Table 5.6: Average volumetric concentration of quartz, kerogen, and calcite in the solid part of the rock for each rock type in the upper depth section of Well B2.

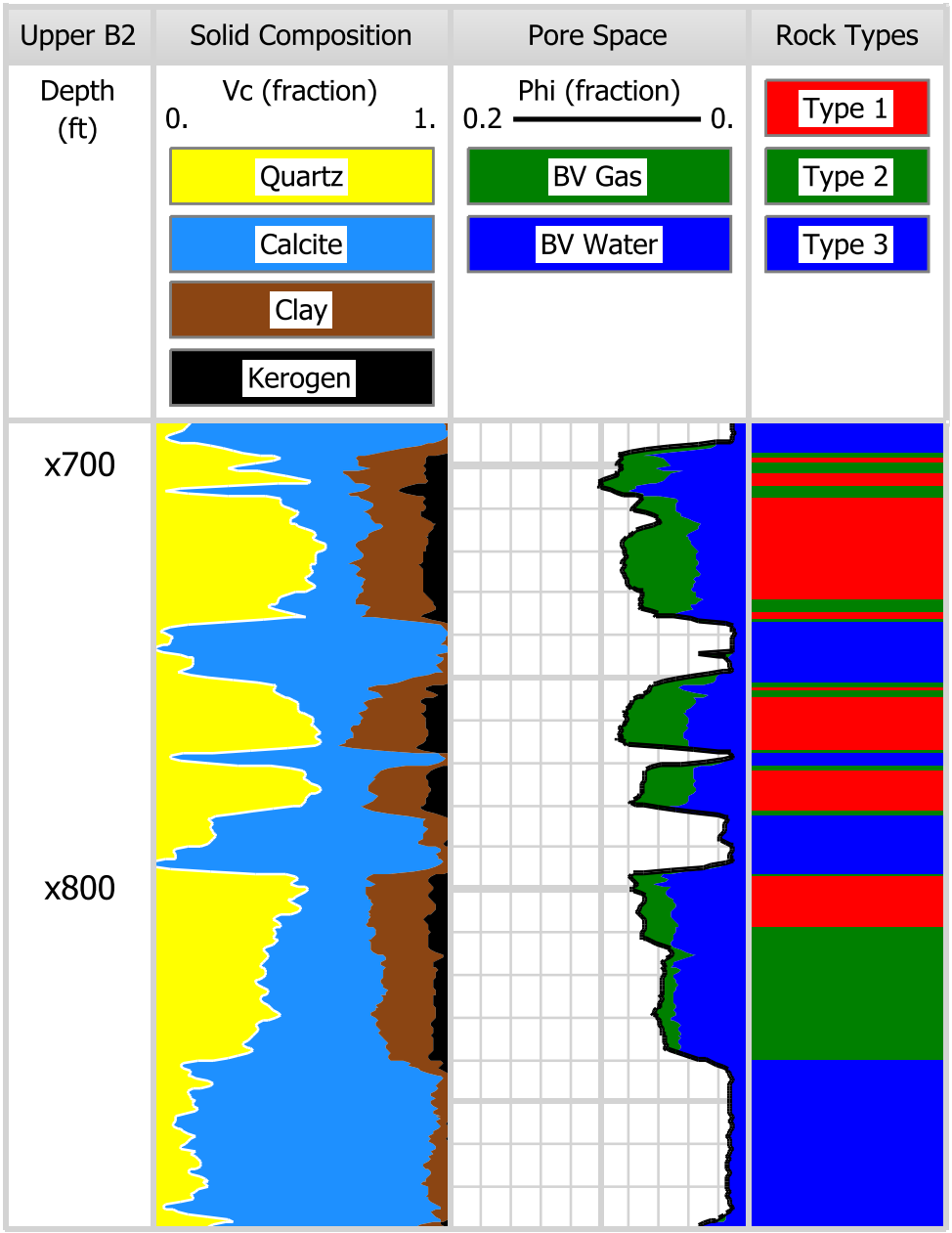

Figure 5.6: Rock typing based on mineral composition in the upper depth section of Well B2. Track 1: relative depth. Track 2: volumetric composition (Vc) of the solid part of the rock. Track 3: porosity and bulk volume (BV) of water and gas. Track 4: rock types.

Figure 5.7 shows the inferred rock composition and rock types in the lower depth section of Well B2, which is thicker than the upper section. Calcite volumetric concentration is high in the top part (average volumetric concentration of calcite from x300 ft to x555 ft is equal to 46%) and decreases with depth. Volumetric concentration of silica and organic matter are larger than in the upper section (average volumetric concentrations of quartz and kerogen in the lower section are equal to 46% and 6%, respectively; they are equal to 31% and 4.6% in the upper section, respectively). Organic content tends to increase with depth. Water saturation is relatively low (mean value is equal to 34%)—except in the top part, from x300 ft to x340 ft, where average value of water saturation is equal to 75%—and there are several carbonate-rich intervals with low porosity, usually water-saturated. Three rock types were identified based on the volumetric concentrations of quartz, calcite, and kerogen. Table 5.7 describes the average volumetric concentration of these constituents in the solid phase of the rock for each rock type. Rock types in the lower depth section are similar to the ones identified in the upper section but are more spatially variable, except in the lower part, where Rock type 1 becomes dominant.

	Quartz	**Kerogen**	**Calcite**
Rock Type 1	55%	9%	15%
Rock Type 2	44%	4%	42%
Rock Type 3	16%	0.8%	81%

Table 5.7: Average volumetric concentration of quartz, kerogen, and calcite in the solid part of the rock for each rock type in the lower depth section of Well B2.

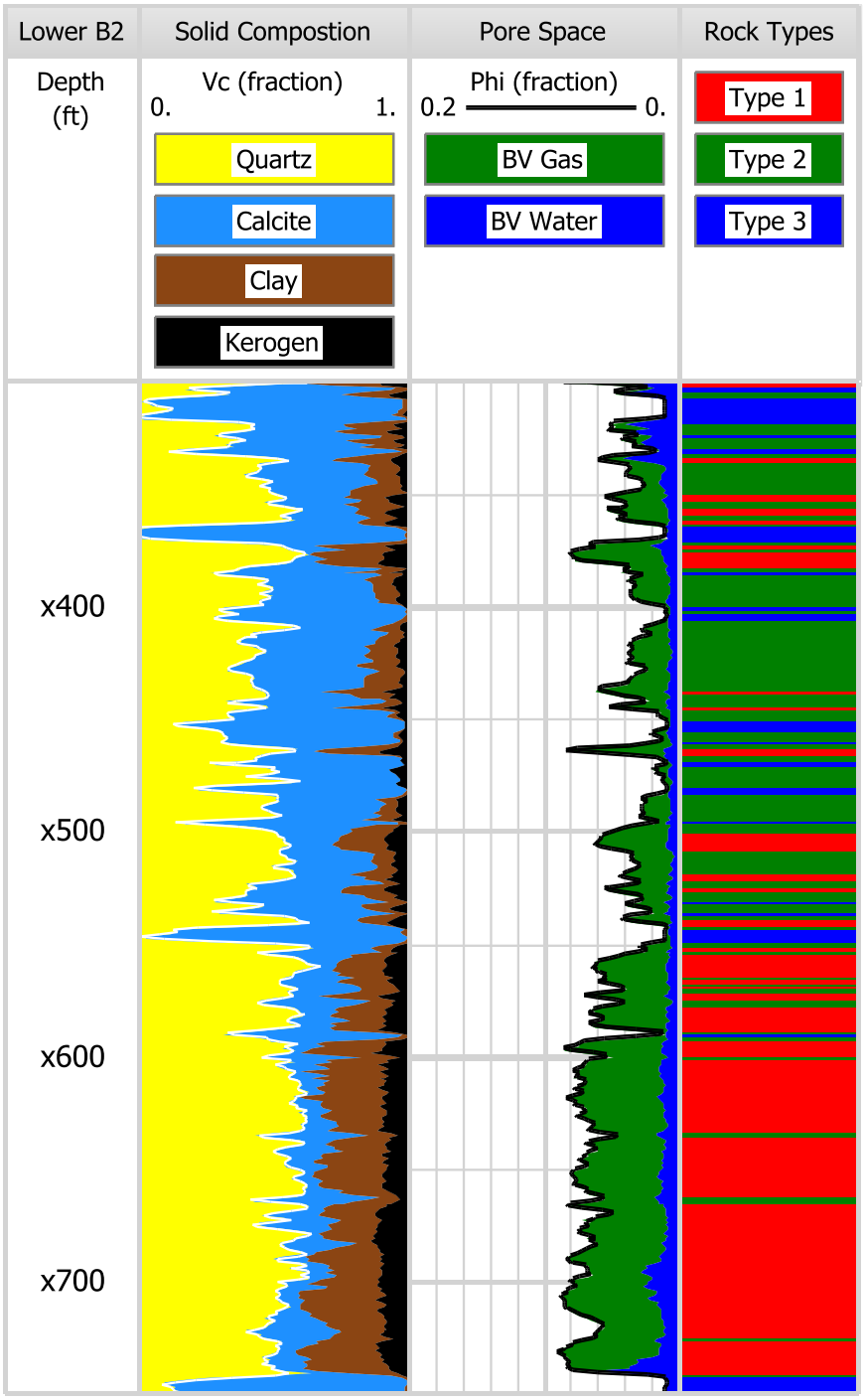
Lower B2
Solid Compostion
Pore Space
Rock Types
Depth (ft)
Vc (fraction)
0.
1.
Quartz
Calcite
Clay
Kerogen
Phi (fraction)
0.2
0.
BV Gas
BV Water
Type 1
Type 2
Type 3
x400
x500
x600
x700

Figure 5.7: Rock typing based on mineral composition in the lower depth section of Well B2. Track 1: relative depth. Track 2: volumetric composition (Vc) of the solid part of the rock. Track 3: porosity and bulk volume (BV) of water and gas. Track 4: rock types.

5.3.2 Analysis of fractures

Drilling-induced fractures are identified in both upper and lower depth sections of Well B2. Electric images also indicate presence of natural fractures. Figure 5.8 shows a 55-ft interval from the lower depth section of Well B2 where both types of fractures are identified on electric images. Rock type 3 contains fewer natural fractures than Rock types 1 and 2 although natural fractures are identified in all rock types along the depth interval of interest. Drilling-induced fractures are identified by discontinuous dark oblique streaks—in this example, electric images get darker as apparent resistivity decreases—. Furthermore, natural fractures are identified by continuous sinusoidal patterns around the borehole. The sinusoidal patterns indicate that natural fractures are nearly vertical, with some dip.

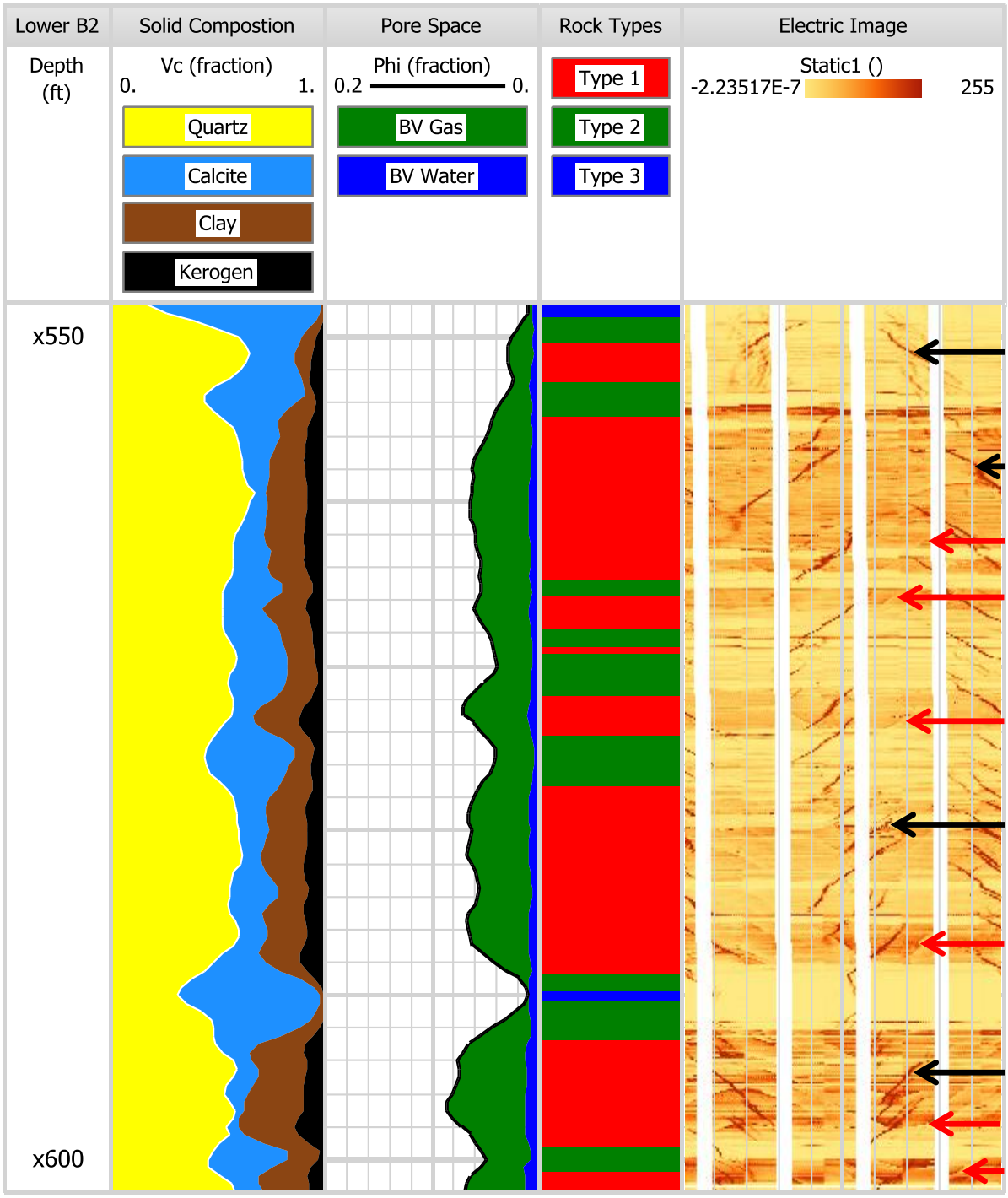
Lower B2
Solid Compostion
Pore Space
Rock Types
Electric Image
Depth (ft)
Vc (fraction)
0.
1.
Quartz
Calcite
Clay
Kerogen
Phi (fraction)
0.2
0.
BV Gas
BV Water
Type 1
Type 2
Type 3
Static1 ()
-2.23517E-7
255
x550
x600

Figure 5.8: Fracture identification in the lower depth section of Well B2. Track 1: relative depth. Track 2: volumetric composition (Vc) of the solid part of the rock. Track 3: porosity and bulk volume (BV) of water and gas. Track 4: rock types. Track 5: electric images. Black and red arrows identify examples of drilling-induced and natural fractures, respectively.

5.3.3 Rock physics model

The isotropic part of the rock is modeled with the DEM. Tables 5.8 and 5.9 describe the corresponding host components and orders in which rock constituents are added to the background matrix for the upper and lower depth sections of Well B2, respectively.

	Rock Type 1	**Rock Type 2**	**Rock Type 3**
Host	Clay	Clay	Calcite
1st inclusion	Kerogen	Kerogen	Quartz
2nd inclusion	Quartz	Calcite	Clay (aspect ratio: 0.01)
3rd inclusion	Calcite	Quartz	Kerogen
4th inclusion	Porosity (aspect ratio: 0.1)	Porosity (aspect ratio: 0.1)	Porosity (aspect ratio: 0.1)

Table 5.8: Host and order of inclusion for each rock type in the upper depth section of Well B2. Inclusions with a given aspect ratio have ellipsoidal shapes. Other inclusions have spherical shapes.

	Rock Type 1	Rock Type 2	Rock Type 3
Host	Clay	Clay	Calcite
1st inclusion	Kerogen	Kerogen	Quartz
2nd inclusion	Quartz	Calcite (aspect ratio: 0.1)	Clay (aspect ratio: 0.01)
3rd inclusion	Calcite	Quartz	Kerogen
4th inclusion	Porosity (aspect ratio: 0.2)	Porosity (aspect ratio: 0.07)	Porosity (aspect ratio: 0.1)

Table 5.9: Host and order of inclusion for each rock type in the lower depth section of Well B2. Inclusions with a given aspect ratio have ellipsoidal shapes. Other inclusions have spherical shapes.

In order to model vertical natural fractures, a fraction of porosity is assumed in the form of vertical cracks with Hudson's model. Tables 5.10 and 5.11 describe fractions of porosity modeled as vertical fractures and their aspect ratio (an ellipsoidal shape is assumed in the simulations) for the upper and lower sections of Well B2, respectively.

	Rock Type 1	Rock Type 2	Rock Type 3
Percentage of the porosity modeled as vertical cracks	15%	20%	10%
Aspect ratio of the vertical cracks	0.1	0.1	0.1

Table 5.10: Percentage of porosity modeled as vertical cracks and fracture aspect ratio in the upper depth section of Well B2.

	Rock Type 1	Rock Type 2	Rock Type 3
Percentage of the porosity modeled as vertical cracks	12%	20%	10%
Aspect ratio of the vertical cracks	0.1	0.1	0.1

Table 5.11: Percentage of porosity modeled as vertical cracks and fracture aspect ratio in the lower depth section of Well B2.

5.3.4 Simulation results

Figures 5.9 and 5.10 describes the calculated velocities—compressional and pure shear—, for the cases of non-averaged and spatially averaged estimations, in the upper

and lower section of Well B2, respectively. Estimated velocities, both non-averaged and spatially averaged, describe velocities of propagation in the vertical direction. Tables 5.12 and 5.13 describe the mean and median of relative errors between averaged estimated and measured velocities, for the upper and lower depth sections of Well B2, respectively.

Means and medians of relative errors are below 4%. The rock physics model reproduces sonic logs accurately, except in a few depth intervals. In the upper depth section, the compressional velocity log exhibits two sharp variations, at x740 ft and x745 ft, that are not reproduced in the simulations. At these depths, the shear velocity does not exhibit a similar behavior; it could suggest that compressional-wave velocity measurements at these depths are not reliable. In the lower depth section, compressional and shear velocities are overestimated at x400 ft, x452 ft, and from x465 ft to x483 ft. Estimated porosity in these three depth intervals is low—less than 2% in average—and may cause simulation errors.

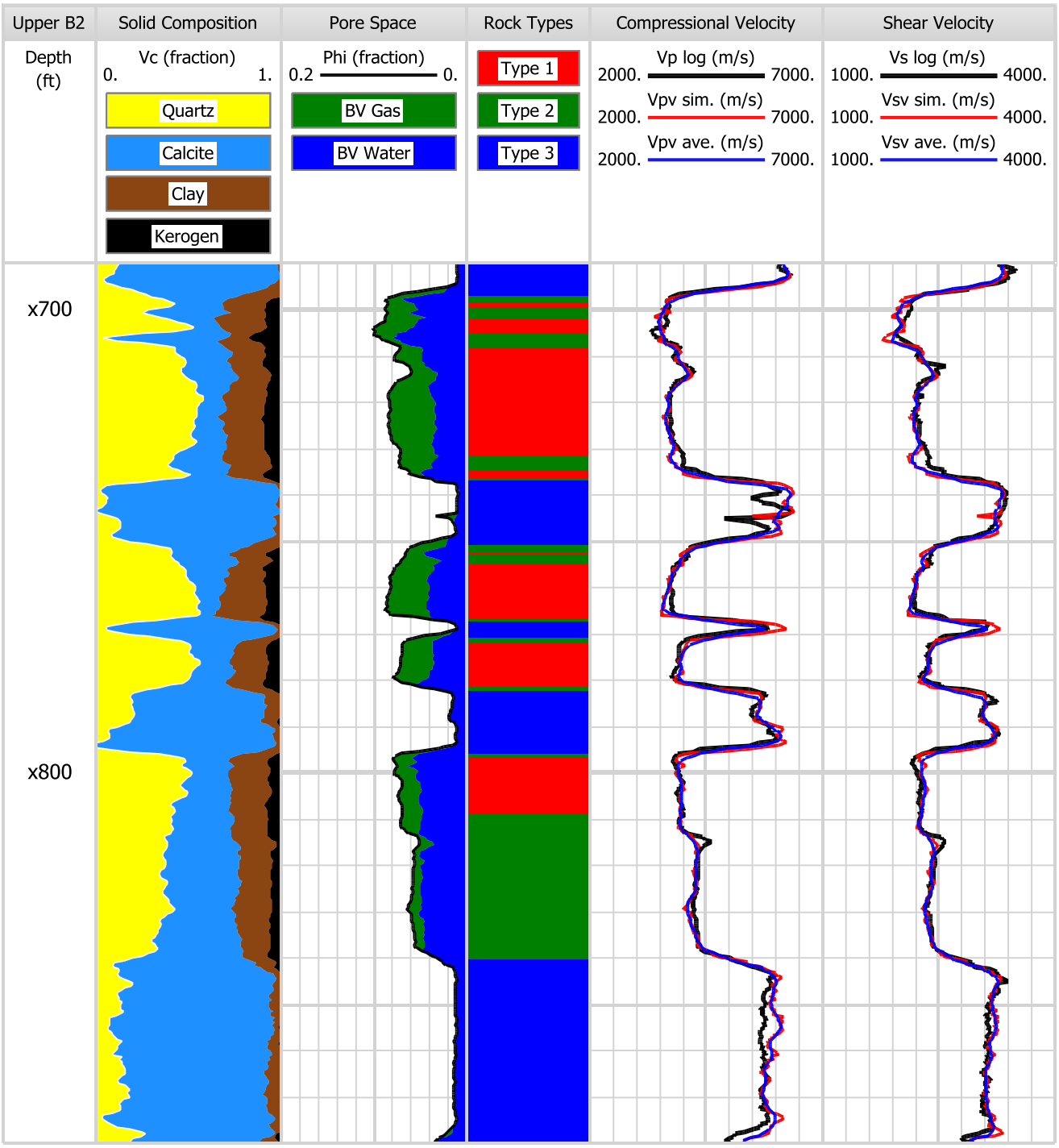
Upper B2
Solid Composition
Pore Space
Rock Types
Compressional Velocity
Shear Velocity
Depth (ft)
Vc (fraction)
0.
1.
Quartz
Calcite
Clay
Kerogen
Phi (fraction)
0.2
0.
BV Gas
BV Water
Type 1
Type 2
Type 3
Vp log (m/s)
2000.
7000.
Vpv sim. (m/s)
2000.
7000.
Vpv ave. (m/s)
2000.
7000.
Vs log (m/s)
1000.
4000.
Vsv sim. (m/s)
1000.
4000.
Vsv ave. (m/s)
1000.
4000.
x700
x800

Figure 5.9: Anisotropic velocity estimation in the upper depth section of Well B2. Track 1: relative depth. Track 2: volumetric composition (Vc) of the solid part of the rock. Track 3: porosity and bulk volume (BV) of water and gas. Track 4: rock types. Track 5: compressional velocity. Track 6: shear velocity. In tracks 5 and 6, black, red, and blue curves identify field, non-averaged estimated, and spatially averaged estimated velocity, respectively. Table 5.12 describes comparison between estimated and measured velocities.

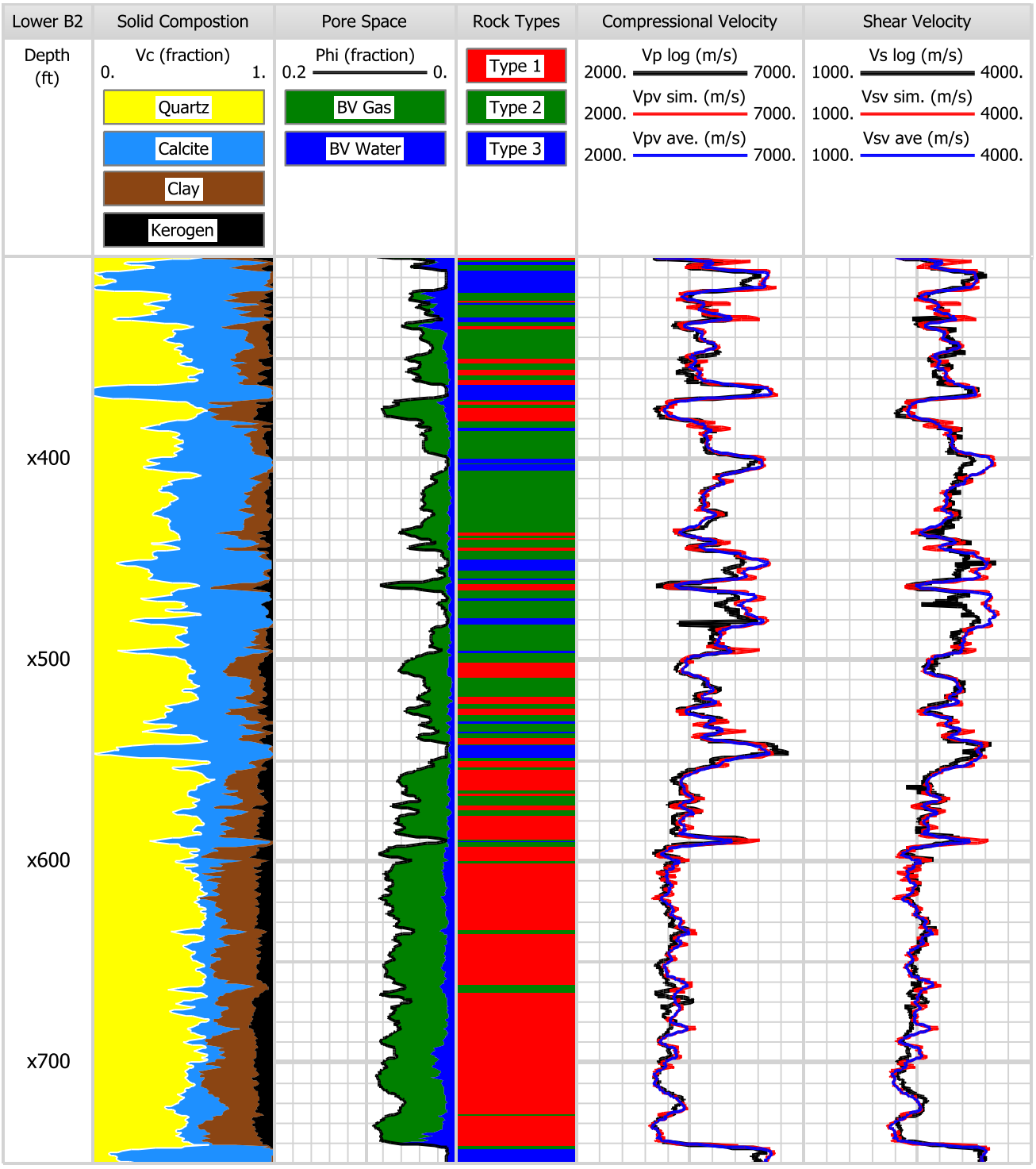
Lower B2
Solid Compostion
Pore Space
Rock Types
Compressional Velocity
Shear Velocity
Depth (ft)
Vc (fraction)
0.
1.
Quartz
Calcite
Clay
Kerogen
Phi (fraction)
0.2
0.
BV Gas
BV Water
Type 1
Type 2
Type 3
Vp log (m/s)
2000.
7000.
Vpv sim. (m/s)
2000.
7000.
Vpv ave. (m/s)
2000.
7000.
Vs log (m/s)
1000.
4000.
Vsv sim. (m/s)
1000.
4000.
Vsv ave (m/s)
1000.
4000.
x400
x500
x600
x700

Figure 5.10: Anisotropic velocity estimation in the lower depth section of Well B2. Track 1: relative depth. Track 2: volumetric composition (Vc) of the solid part of the rock. Track 3: porosity and bulk volume (BV) of water and gas. Track 4: rock types. Track 5: compressional velocity. Track 6: shear velocity. In tracks 5 and 6, black, red, and blue curves identify field, non-averaged estimated, and averaged estimated velocity, respectively. Table 5.13 describes comparison between simulated and field velocities.

	Compressional Velocity	Shear Velocity
Mean of relative errors	3.23%	2.36%
Median of relative errors	2.61%	1.84%

Table 5.12: Mean and median of relative errors between spatially averaged anisotropic estimated and measured velocities in the upper depth section of Well B2.

	Compressional Velocity	Shear Velocity
Mean of relative errors	3.79%	3.13%
Median of relative errors	3.59%	2.69%

Table 5.13: Mean and median of relative errors between spatially averaged anisotropic estimated and measured velocities in the lower depth section of Well B2.

5.3.5 Interpretation of results

Even though the upper and lower depth sections of Well B2 are separated by a limestone formation, their rock types are analogous and exhibit similar rock fabric properties. Rock type 2 exhibits the largest fraction of porosity in the form of vertical cracks. Although natural fractures may enhance fluid flow, they are not suitable for hydraulic stimulation because they could absorb fracturing energy and therefore prevent tree-like growth of new fractures. Rock type 1 exhibits the largest volumetric concentrations of quartz and kerogen. It also contains less porosity in the form of vertical fractures than Rock type 2. Therefore, depth intervals with Rock type 1 are assumed to be the most suitable for production and become preferential targets for hydraulic stimulation. Depth intervals with Rock type 1 or 2 that are connected to a water-bearing zone should be avoided because of risk of water production through natural fractures. Rock type 3 exhibits low porosity and large volumetric concentration of calcite; with calcite as load-bearing material, it is the stiffest rock type. Rocks within this category are the most likely to confine fracture propagation. They are also the most reliable for horizontal well placement because they are more resistant to collapse than Rock types 1 and 2.

Depth intervals with Rock type 3 at x745 ft and x790 ft in the upper depth section of Well B2 are suitable targets for horizontal well placement. They exhibit a strong frame and favorable exposure to hydrocarbon-rich zones with Rock types 1 and 2, above and below. The depth interval from x550 ft to x740 ft in the lower section of Well B2 is the most interesting for production because of high porosity, high gas saturation, and large volumetric concentration of organic matter. Carbonate layers at x590 ft and x545 ft are suitable for drilling a horizontal well, even though the first one may be a difficult target for drillers because of its relatively small thickness. Both of these intervals exhibit a

strong frame and favorable exposure to hydrocarbon-rich zones, above and below. The carbonate layer at x750 ft does not seem to contain natural fractures. Therefore, it is likely to prevent hydraulic fractures from propagating below the Barnett shale. Hydrocarbons above x550 ft could be produced from a well drilled in the depth interval with Rock type 3 at x450 ft. However, abundance of Rock type 3 layers in this interval may prevent long-reach fracture propagation. Moreover, smaller hydrocarbon content than in the lower depth section of the well—below x550 ft—makes this zone less favorable for production.

5.4 SUMMARY

Different rock physics model are invoked in the two wells. This condition indicates that the rock fabric of the Barnett shale is likely to be laterally heterogeneous. Therefore, rock fabric properties and rock physics models in the Barnett shale should be extrapolated from one well to another with caution. Rock typing is required in the two wells to accurately reproduce sonic measurements. It suggests that both Well B1 and B2 exhibit a vertically heterogeneous rock fabric. Horizontal compliant pores and calcareous shells are modeled in Well B1. Combination of large volumes of organic matter and compaction stress is assumed to be the main cause for partial horizontal distribution of pores. Natural fractures are identified in Well B2. Unlike in the case of the Haynesville shale, the Barnett shale rock fabric properties are vertically heterogeneous. Therefore, identification of suitable rock types for drilling horizontal wells and intervals to initiate or contain fracture propagation is based on rock fabric. Rock physics models in the Barnett shale are anisotropic. Consequently, the Young's modulus and Poisson's ratio are not used in the interpretations.

Chapter 6: Conclusion

Based on rock composition and sonic/density logs, a simulation method and corresponding interpretation technique were developed to quantify rock fabric properties in hydrocarbon-bearing organic shales,. Rock physics models were invoked to model rock elastic properties of formations with specific fabric attributes: load-bearing matrix, constituent shapes, anisotropic cracks, and spatial heterogeneity. Estimated velocities were compared to measured compressional- and shear-wave velocities to validate rock fabric properties. The method was tested in the Haynesville and Barnett shales. Rock physics models are different from one formation to another, reflecting differences in rock fabric.

6.1 Haynesville Shale

Compressional and shear velocity logs were accurately reproduced: averages of relative errors between estimated and measured velocities were less than 4% in the two wells. Isotropic modeling was reliable for the numerical simulation of sonic logs. Anisotropy between vertical and horizontal elastic properties could primarily result from other factors, such as stress, for instance. An identical rock fabric was assumed for the entire depth interval in the two wells, from the bottom of the Bossier shale to the top of the Haynesville limestone. Therefore, rock fabric in this region of the Haynesville shale is likely to be vertically homogeneous. The load-bearing matrix is also shown to be constituted of clay. The same rock fabric is invoked in the two wells and measured velocities are accurately reproduced in the simulations. It suggests that rock fabric is laterally homogeneous in such a region of the Haynesville shale. The only parameter that

was refined was the pore aspect ratio. Well H2 exhibited a smaller pore aspect ratio and is deeper than Well H1. It indicates that compaction could drive pore shape.

Suitable depth intervals for horizontal well placement in Wells H1 and H2 were identified in the middle of the Hayneville shale. These intervals exhibit high velocities, high Young's modulus, and good exposure to hydrocarbon-rich zones above and below—with high porosity and gas saturation—. The calcite-rich Haynesville limestone represents a natural fracture containment obstacle, as does the Bossier shale. Therefore, there is little risk of accidentally stimulating non-suitable intervals, either above or below the Haynesville shale. Estimations of Poisson's ratio did not accurately reproduce Poisson's ratio calculated from sonic/density logs. Poisson's ratio was shown to be more sensitive to measurement errors than Young's modulus and was therefore deemed not suitable for interpretation.

6.2 BARNETT SHALE

Well B1 is located in the south/southwestern region of the Barnett shale, whereas Well B2 is located in the north/northeastern region. Well B2 was divided into two depth intervals: upper and lower sections. Each well was divided into layers with similar rock composition. Five rock types were identified in Well B1 whereas three rock types were identified in the two depth sections of Well B2. Specific rock fabric properties were invoked for each rock type, indicating that rock fabric in the Barnett shale is vertically heterogeneous.

Isotropic models did not reproduce sonic logs reliably, whereby Hudson's model was invoked to model the anisotropic distribution of some rock components. Different anisotropic properties were used in the two wells.

Rock types and rock physics models are different from one well to the other. Therefore, rock fabric in the Barnett shale is likely to by laterally heterogeneous. Extrapolation of a rock physics model from one well to another in the Barnett shale should be done with caution, especially if the wells are not within the same geological demarcation zone.

6.2.1 Well B1

Sonic logs were reliably reproduced with an anisotropic rock physics model: averages of relative errors between estimated and measured velocities were less than 4%. Clay is the dominant load-bearing constituent, (except for Rock type 2 where kerogen was chosen as load-bearing), mixed with kerogen for Rock types 1 and 4 and with quartz for Rock type 5. Horizontal compliant cracks were modeled in Well B1. This type of pore shape may be due to large volumetric concentration of soft organic matter. Because of the softness of the rock, pores deform under the influence of overburden stress. This phenomenon may be influenced by the geometric configuration of horizontal carbonate shells. A Rock type 3 depth interval in the middle of the formation, at x770 ft, was shown to represent the most suitable location to drill a horizontal well. It exhibits large amounts of both silica and calcite and high sonic velocities. It is bounded by hydrocarbon- and organic-rich rocks and is located far from stiff layers present at the top and bottom of this section of the Barnett shale, which could contain vertical fracture propagation.

6.2.2 Well B2

In Well B2, both in the upper and lower sections, electric images indicated presence of natural vertical fractures. The effect of these fractures on formation elastic

properties was accounted for when using Hudson's model to add vertical cracks. Sonic logs were reliably reproduced with this procedure: averages of relative errors between estimated and measured velocities were less than 4%. Rock types exhibit different numbers of natural fractures, which may indicate that the formation of such cracks could be affected by rock composition (given that rock typing was based on rock composition). Because natural fractures tend to absorb energy from hydraulic stimulation, Rock type 1 was preferred over Rock type 2 for performing hydraulic stimulation (the fraction of porosity in the form of fractures is lower in rock type 1). Rock type 3 was identified as the most suitable Rock type to place a horizontal well as the calcite load-bearing matrix is likely to provide a good resistance to collapse. Load-bearing matrix for Rock types 1 and 2 was shown to be composed of clay.

Identification of suitable zones for horizontal well placement in the upper depth section of Well B2 was based on calcite volumetric concentration and velocities. Two depth intervals, at x745 ft and x790 ft, were identified as suitable for drilling a horizontal well. They exhibit large volumetric concentrations of calcite, which provide stability and resistance to collapse, and are bounded by favorable rocks for production. These suitable rocks for production exhibit high porosity and high gas saturation.

The lower depth section of Well B2 is more vertically heterogeneous than the upper one. On the basis of porosity, gas saturation, and organic content, the best production interval was identified between x550 ft and x740 ft. In this interval, the carbonate layer of rock type 3 at x590 ft was identified as the most suitable location for drilling a horizontal well. It exhibits calcite load-bearing matrix, low clay volumetric concentration, low porosity, and high velocities.

6.3 SUGGESTIONS FOR FUTURE WORK

Because parameters such as stress, pore pressure, and temperature affect rock elastic properties, it would be valuable to integrate these properties in a more advanced rock physics model. Quantification of in-situ stress is critical for optimum fracture stimulation design. Pore pressure is also an important formation property. Quantifying the impact of pore pressure on elastic properties would provide, for instance, information on how the rock will be mechanically affected by fluid depletion after well completion. Temperature affects elastic properties of minerals, especially clay. Although its impact on in-situ rock elastic properties is likely to be negligible compared the one of stress and pore pressure, quantification of temperature effect on rock mechanical properties would be valuable when comparing core measurements to well logs.

Similar minerals were grouped during inversion for estimation of rock composition. For example, dolomite was grouped with calcite into a single component; a similar process was invoked for different types of clay minerals. Secondary minerals (which are grouped with a mineral of higher concentration; dolomite is grouped with calcite, for example) may have different elastic properties compared to the main mineral with which they were grouped. More accurate estimations of rock composition, without grouping, will limit input errors and enable a more reliable assessment of rock fabric properties.

Given the larger number of inputs compared to outputs, quantification of rock fabric properties involves a non-unique estimation problem. More field data are necessary to reduce the number of solutions. Complete quantification of elastic tensors, for example, is possible with core elastic properties measurements. However, in that case, one must be aware that mechanical properties of cores brought to the surface may differ from in-situ formation elastic properties.

Appendix: First-Order Correction Coefficients in Hudson's Model

Hudson's model (1980) is based on a scattering theory and describes the effect of oriented ellipsoidal inclusions, or cracks, in an isotropic background medium on rock elastic properties. This rock physics model is used to quantify the degree of anisotropy of rock matrix. This section is intended to describe the formulation of first-order corrections applied to the entries of the isotropic background stiffness tensor. Only first-order correction is used because second-order correction can lead to convergence problems (Cheng, 1993).

First-order correction coefficients for a set of cracks aligned normally along the 3-axis are given by

$$c_{11}^{1} = -\frac{{\lambda_m}^2}{\mu_m}\varepsilon_{crack}U_3,$$

$$c_{13}^{1} = -\frac{\lambda_m(\lambda_m + 2\mu_m)}{\mu_m}\varepsilon_{crack}U_3,$$

$$c_{33}^{1} = -\frac{(\lambda_m + 2\mu_m)^2}{\mu_m}\varepsilon_{crack}U_3,$$

$$c_{44}^{1} = -\mu_m\varepsilon_{crack}U_1,$$

and

$$c_{66}^{1} = 0,$$

where

$$\varepsilon_{crack} = \frac{3x_{crack}}{4\pi\alpha_{crack}},$$

and

$$\lambda_m = K_m - \frac{2}{3}\mu_m.$$

For dry cracks, U_1 and U_3 are defined by

$$U_1 = \frac{16(\lambda_m + 2\mu_m)}{3(3\lambda_m + 4\mu_m)},$$

and

$$U_3 = \frac{4(\lambda_m + 2\mu_m)}{3(\lambda_m + \mu_m)}.$$

For other cracks (referred to as inclusions, for which elastic moduli are not zero), U_1 and U_3 are defined by

$$U_1 = \frac{16(\lambda_m + 2\mu_m)}{3(3\lambda_m + 4\mu_m)}\frac{1}{(1+\chi)},$$

and

$$U_3 = \frac{4(\lambda_m + 2\mu_m)}{3(\lambda_m + \mu_m)}\frac{1}{(1+\kappa)}.$$

where

$$\chi = \frac{4\mu'}{\pi\alpha_{crack}\mu_m}\frac{(\lambda_m + 2\mu_m)}{(3\lambda_m + 4\mu_m)},$$

and

$$\kappa = \frac{(K' + \frac{4}{3}\mu')(\lambda_m + 2\mu_m)}{\pi\alpha_{crack}\mu_m(\lambda_m + \mu_m)}.$$

In the above expressions, K_m and μ_m are the bulk and shear moduli of the isotropic background, respectively; α_{crack} and x_{crack} describe crack (or inclusion) aspect ratio and volumetric concentration, respectively. For inclusions with non-zero elastic moduli, *K'* and *u'* designate their bulk and shear moduli, respectively.

Nomenclature

c_{ijkl} : Element of elastic stiffness tensor, [GPa]

c_{ijkl}^{dry} : Element of elastic stiffness tensor of the dry transverse isotropic rock, [GPa]

c_{ijkl}^{sat} : Element of elastic stiffness tensor of the saturated transverse isotropic rock, [GPa]

c_{IJ} : Element of elastic stiffness tensor in Voigt's notation, [GPa]

c_{ijkl}^{eff} : Element of elastic stiffness tensor of the effective transverse isotropic medium in Hudson's model, in Voigt's notation, [GPa]

c_{ijkl}^{0} : Element of elastic stiffness tensor of the background isotropic medium in Hudson's model, in Voigt's notation, [GPa]

c_{ijkl}^{1} : Element of elastic stiffness tensor of the first-order correction in Hudson's model, in Voigt's notation, [GPa]

c_{ijkl}^{2} : Element of elastic stiffness tensor of the second-order correction in Hudson's model, in Voigt's notation, [GPa]

E : Young's modulus, [GPa]

K : Bulk modulus, [GPa]

K^{ave_V} : Vertically-averaged effective bulk modulus of the rock, [GPa]

K_{dry} : Bulk modulus of the dry isotropic rock, [GPa]

K^{eq_V} : Vertical effective bulk modulus of the rock, [GPa]

K_{flu} : Bulk modulus of the fluid mixture, [GPa]

K_g : Bulk modulus of gas, [GPa]

K_i : Bulk modulus of the *i*-th inclusion, [GPa]

K_m : Bulk modulus of the isotropic medium, [GPa]

K_{sat} : Bulk modulus of the saturated isotropic rock, [GPa]

K_w : Bulk modulus of water, [GPa]

K_0 : Bulk modulus of the isotropic solid mixture, [GPa]

K_1 : Bulk modulus of the host material in the differential effective medium theory, [GPa]

K_2 : Bulk modulus of the inclusion material in the differential effective medium theory, [GPa]

K' : Bulk modulus of the anisotropic inclusion in Hudson's model, [GPa]

K^*_{SC} : Bulk modulus of the background medium in the self-consistent approximation, [GPa]

K^*_{DEM} : Bulk modulus of the background medium in the differential effective medium theory, [GPa]

N : Number of phases in a mixture, []

N_L : Number of layers for vertical averaging of rock properties, []

P : Geometric coefficient in the Self-Consistent Approximation and the Differential Effective Model, []

Q : Geometric coefficient in the Self-Consistent Approximation and the Differential Effective Model, []

V_P : Velocity of the compressional wave in an isotropic medium, [m/s]

$V_{PS\ TI}$: Velocity of the pure shear wave in a transverse isotropic medium, [m/s]

V_{PV} : Vertical velocity of the compressional wave, [m/s]

$V_{PV\ ave}$: Vertically-averaged velocity of the compressional wave, [m/s]

$V_{P\ TI}$: Velocity of the compressional wave in a transverse isotropic medium, [m/s]

$V_{QS\ TI}$: Velocity of the quasi-shear wave in a transverse isotropic medium, [m/s]

V_S : Velocity of the shear wave in an isotropic medium, [m/s]

V_{SV} : Vertical velocity of the shear wave, [m/s]

$V_{SV\ ave}$: Vertically-averaged velocity of the shear wave, [m/s]

s_w : Water saturation, []

x_{crack} : Volumetric concentration of cracks in Hudson's model, []

x_i : Volumetric concentration of the *i*-th phase in a mixture, []

x_2 : Volumetric concentration of the inclusion material in the differential effective medium theory, []

α : Aspect ratio of an element with ellipsoidal shape, []

α_{crack} : Crack aspect ratio in Hudson's model, []

α_i : Aspect ratio of the *i*-th inclusion, []

ε_{crack} : Crack density in Hudson's model, []

ε_{kl} : Element of strain tensor, []

μ : Shear modulus, [GPa]

μ^{ave_V} : Vertically-averaged effective shear modulus of the rock, [GPa]

μ^{eq_V} : Vertical effective shear modulus of the rock, [GPa]

μ_i : Shear modulus of the *i*-th inclusion, [GPa]

μ_m : Shear modulus of the isotropic medium, [GPa]

μ_1 : Shear modulus of the host material in the differential effective medium theory, [GPa]

μ_2 : Shear modulus of the inclusion material in the differential effective medium theory, [GPa]

μ' : Shear modulus of the anisotropic inclusion in Hudson's model, [GPa]

μ^*_{SC} : Shear modulus of the background medium in the self-consistent approximation, [GPa]

μ^*_{DEM} : Shear modulus of the background medium in the differential effective medium theory, [GPa]

υ : Poisson's ratio, []

Φ : Total porosity, []

ρ : Bulk density, [g/cm^3]

ρ^{ave_V} : Vertically averaged bulk density of the rock, [GPa]

ρ_b : Rock bulk density, [g/cm^3]

ρ_l : Bulk density of the l-th layer in vertical averaging of rock properties, [g/cm^3]

σ_{ij} : Element of stress tensor, [GPa]

θ : Angle between acoustic wave direction of propagation and x_3-axis of symmetry in a transverse isotropic medium, []

Acronyms

AT	:	Two-Feet Array-Induction Log
AO	:	One-Foot Array-Induction Log
BV	:	Bulk Volume
DEM	:	Differential Effective Medium
DRho	:	Delta-Density Log
FERC	:	Federal Energy Regulatory Commission
gAPI	:	American Petroleum Institute Gamma-ray Units
GR	:	Natural Gamma-Ray Log
LS	:	Limestone Unit for Neutron Porosity Log
PhiN	:	Neutron Porosity Log
Rhob	:	Bulk Density Log
SCA	:	Self-Consistent Approximation
Vc	:	Volumetric Concentration of Rock Constituents in the Solid Part of the Rock
XRD	:	X-Ray Diffraction

References

Adiguna, H., 2012, Comparative Study for the Interpretation of Mineral Concentrations, Total Porosity, and TOC in Hydrocarbon-Bearing Shale from Conventional Well Logs, Master's Thesis, The University of Texas at Austin.

Ahmadov, R., Vanorio, T., and Mavko, G., 2009, Confocal laser scanning and atomic-force microscopy in estimation of elastic properties of the organic-rich Bazhenov formation, *The Leading Edge*, 28, 18-23.

Backus, G. E., 1962. Long-wave elastic anisotropy produced by horizontal layering, *Journal of Geophysical Research*, 67, 4427-4440.

Berryman, J. G., 1980, Confirmation of Biot's theory, *Applied Physics Letters*, 37, 382-384.

Berryman, J. G., 1980, Long-wavelength propagation in composite elastic media, *Journal of Acoustic Society of America*, 69, 1809-1831.

Berryman, J. G., 1992, Single-scattering approximations for coefficients in Biot's equations of poroelasticity, *Journal of Acoustic Society of America*, 91, 551-571.

Berryman, J. G., 1995, Mixture theories for rock properties, *Rock Physics and Phase Relations: a Handbook of Physical Constants*, ed. T.J. Ahrens. Washington, DC: American Geophysical Union, pp. 205-228.

Biot, M. A., 1956, Theory of propagation of elastic waves in a fluid saturated porous solid. I: Low frequency range, and II: Higher-frequency range, *Journal of Acoustic Society of America*, 28, 168-191.

Britt, L., and Schoeffler, J., 2009, The geomechanics of a shale play: What makes a shale prospective!, *SPE Eastern Regional Meeting*, Charleston, West Virginia, USA, September 23-25.

Bruggeman, D. A. G., 1935, Berechnung verschiedener physikalischer Konstanten von heterogenen Substanzen, *Annalen der Physik*, 24, 636-679.

Budiansky, B.,1965, On the elastic moduli of some heterogeneous materials, *Journal of the Mechanics and Physics of Solids,* 13, 223-227.

Cheng, C. H., 1993, Crack models for a transversely anisotropic medium, *Journal of Geophysical Research*, 98, 675-684.

Gassmann, F., 1951, Über die Elastizität poröser Medien, *Vierteljahrsschrift der Naturforschenden Gesellschaft in Zürich*, 96, 1-23.

Hammes, U., Hamlin, H. S., and Ewing, T. E., 2011, Geologic analysis of the upper Jurassic Haynesville shale in east Texas and west Louisiana, *AAPG Bulletin*, v. 95, no. 10, pp. 1643–1666.

Hashin, Z., and Shtrikman, S., 1963, A variational approach to the elastic behavior of multiphase materials, *Journal of the Mechanics and Physics of Solids*, 11, 127-140.

Heidari, Z., 2011, Estimation of Static and Dynamic Petrophysical Properties from Well Logs in Multi-layer Formations, PhD Dissertation, The University of Texas at Austin.

Hill, R., 1965, A self-consistent mechanics of composite materials, *Journal of the Mechanics and Physics of Solids*, 13, 213-222.

Hornby, B. E., Schwartz, L. M., and Hudson, J. A., 1994, Anisotropic effective-medium modeling of the elastic properties of shales, *Geophysics*, 59, 1570-1583.

Hudson, J. A., 1980, Overall properties of a cracked solid, *Mathematical Proceedings, Cambridge Philosophical Society,* 88, 371-384.

Hudson, J. A., and Liu, E., 1999, Effective elastic properties of heavily faulted structures, *Geophysics*, 64, 479-485.

Jarvie, D. M., Hill, R. J., Ruble, T. E., and Pollastro, R. M., 2007, Unconventional shale-gas systems: The Mississippian Barnett shale of north-central Texas as one model for thermogenic shale-gas assessment, *AAPG Bulletin*, v. 91, no. 4, pp. 475–499.

King, G., 2010, Thirty years of gas shale fracturing: What have we learned?, *SPE Annual Technical Conference and Exhibition*, Florence, Italy, September 19-22.

Kuster, G. T., and Toksöz, M. N., 1974, Velocity and attenuation of seismic waves in two-phase media, *Geophysics*, 39, 587-618.

Mavko, G., Mukerji, T., and Dvorkin, J., 2009, The Rock Physics Handbook, Second Edition: Tools for Seismic Analysis of Porous Media, *Cambridge University Press*.

Montgomery, S. L., Jarvie, D. M., Bowker, K. A., and Pollastro, R. M., 2005, Mississippian Barnett shale, Fort Worth basin, north-central Texas: Gas-shale play with multi–trillion cubic foot potential, *AAPG Bulletin*, v. 89, no. 2, pp. 155–175.

Reuss, A., 1929, Berechnung der Fliessgrenzen von Mischkristallen auf Grung der Plastizitätsbedingung für Einkristalle, *Zeitschrift für Angewandte Mathematik und Mechanik*, 9, 49-58.

Ruiz, F., and Cheng, A., 2010, A rock physics model for tight gas sand, *The Leading Edge*, December, 1484-1488.

Sheng, P., 1990, Effective-medium theory of sedimentary rocks, *Physical Review*, B41, 7, 4507-4512.

Sheng, P., 1991, Consistent modeling of the electrical and elastic properties of sedimentary rocks, *Geophysics*, 56, 1236-1243.

Smith, T. M., Sayers, C. M., and Sondergeld, C. H., 2009, Rock properties in low-porosity/low-permeability sandstones, *The Leading Edge*, January, 48-59.

Sone, H., and Zoback, M. D., 2010, Strength, creep and frictional properties of gas shale reservoir rocks, *American Rock Mechanics Association*.

Vernik, L., and Milovac, J., 2011, Rock physics of organic shales, *The Leading Edge*, March, 318-323.

Wu, T. T., 1966, The effect of inclusion shape on the elastic moduli of a two-phase material, *International Journal of Solids and Structure*, 2, 1-8.

Wyllie, M. R. J., Gregory, A. R., and Gardner, L. W., 1956, Elastic wave velocities in heterogeneous and porous media, *Geophysics*, 21, 41-70.

Wyllie, M. R. J., Gregory, A. R., and Gardner, G. H. F., 1958, An experimental investigation of factors affecting elastic wave velocities in porous media, *Geophysics*, 23,459-493.

Xu, S., and White, R. E., 1995, A new velocity model for clay-sand mixtures, *Geophysical Prospecting*, 43, 91-118.